TIDAL AND PLANETARY WAVES

Jeffrey M. Forbes[1]

High Altitude Observatory, National Center for Atmospheric Research[2]

Boulder, CO, 80307-3000, U.S.A.

A Tutorial Lecture

Chapman Conference on the Mesosphere and Lower Thermosphere

Asilomar, CA, November, 1992

and

The CEDAR Workshop, June, 1993

---

[1] On leave from the Center for Space Physics and Department of Electrical, Computer and Systems Engineering, Boston University, Boston, MA, 02215

[2] The National Center for Atmospheric Research is sponsored by the National Science Foundation

1. INTRODUCTION

Atmospheric tides are global-scale oscillations in temperature, wind, density, and pressure at periods which are subharmonics of a solar or lunar day. Strictly speaking, atmospheric tides may be either eastward- or westward propagating, but by far the largest components are those which are westward-propagating or *migrating* with the apparent motion of the sun or moon. Planetary waves are longer-period global oscillations which are either stationary (i.e., fixed to the earth) or zonally-propagating in either direction. Without intending to diminish the importance of the other wave components, in the interest of brevity the present tutorial will mainly concentrate on westward-propagating solar tides and planetary waves.

A brief view of typical observations provides adequate motivation for the present tutorial. Figure 1 illustrates height/local time contours representing average meridional wind patterns between 80 and 100 km over Townsville, Australia (19°S, 147°E) and Saskatoon, Canada (54°N, 107°W) during the period March 18-27, 1979. Note first of all that the character is mainly diurnal over Townsville (24-hour harmonic dominates), and mainly semidiurnal over Saskatoon (12-hour harmonic dominates). Why do you suppose this is? Why is it that phase progression is downward (i.e., the wind contours tilt to the left in Figure 1)? And, given that there are no significant heat sources at these heights, why is it that these "tidal" oscillations assume such a prominent role in the meteorology of the mesosphere and lower thermosphere?

Instead of the average local time (day/night) wind structure examined in Figure 1, now suppose that we compute the daily mean wind (24-hour average) each day at a single height and form a time series of the daily values. The spectral density curve corresponding to daily mean winds measured over Obninsk, Russia (54°N, 38°E) during January through February, 1979, are illustrated in Figure 2. Note that prominent peaks occur near 5, 9, and 16 days period; a simple band-pass/IFT analysis demonstrates that these peaks each correspond to some 5-10 ms^{-1} oscillation in the wind, a substantial fraction of the total

wind at any given time. Assuming this example is representative, why is it that the spectral peaks should fall at these specific periods?

Perhaps the most well-known long-period oscillation is the so-called two-day wave. A history of 2-day wave amplitudes determined from mesopause winds measured over Adelaide, Australia (35°S, 138°E) is illustrated in Figure 3 [Harris, 1993]. Note that amplitudes of order 20-40 ms^{-1} episodically occur. Why should a prominent oscillation at this period exist near the mesopause?

This tutorial is motivated by the simple fact that tidal and planetary waves often dominate the meteorology of the atmospheric region between 80 and 150 km. Students and scientists engaged in studies of this regime should have some rudimentary understanding of the origins, characteristics, and governing mechanisms pertinent to these oscillations. The present tutorial seeks to impart this basic understanding.

Given that the present work is a tutorial rather than a comprehensive review of research in the field, I have not provided extensive referencing to the huge body of published literature on tidal and planetary waves. Some exceptions are works of historical importance, or recent papers which are particularly illustrative or instructive. For more extensive expositions than provided here, including references to the literature, the reader is referred to Chapman and Lindzen [1970] and Forbes [1982 a,b] for solar and lunar atmospheric tides, and to Walterscheid [1980] and Salby [1984] for traveling planetary waves. There also exists an extensive literature on stationary planetary waves. A recent paper which emphasizes the vertical extension of stationary planetary waves into the mesosphere/lower thermosphere is Pogorel'tsev and Sukhanova [1993].

In the following section, the mathematics governing free and forced oscillations in a horizontally stratified isothermal atmosphere is developed. The resulting analytic solutions provide a reference framework for interpreting observations and numerical simulations. Anticipated modifications to this simple theory due to non-isothermality, mean winds, and dissipation are also discussed. Thermal forcing of atmospheric tides is covered in Section

3. In Section 4 several examples of numerical simulations of tidal and planetary waves are presented and interpreted. A brief outlook of potentially fruitful areas of research is provided in Section 5.

2. MATHEMATICAL BASIS

2.1 Governing Equations

In the absence of mean winds, the *linearized* equations for atmospheric perturbations on a sphere are [Holton, 1975]:

$$\frac{\partial u}{\partial t} - 2\Omega \sin\theta v + \frac{1}{a\cos\theta}\frac{\partial \Phi}{\partial \lambda} = 0 \tag{1}$$

$$\frac{\partial v}{\partial t} + 2\Omega \sin\theta u + \frac{1}{a}\frac{\partial \Phi}{\partial \theta} = 0 \tag{2}$$

$$\frac{\partial}{\partial t}\Phi_z + N^2 w = \frac{\kappa J}{H} \tag{3}$$

$$\frac{1}{a\cos\theta}\left[\frac{\partial u}{\partial \lambda} + \frac{\partial}{\partial \theta}(v\cos\theta)\right] + \frac{1}{\rho_o}\frac{\partial}{\partial z}(\rho_o w) = 0 \tag{4}$$

u = eastward velocity

v = northward velocity

Φ = geopotential

$w = dz/dt$

N^2 = buoyancy frequency squared

Ω = angular velocity of earth

ρ_o = basic state density

$z = -H ln(p/p_o)$

λ = longitude

θ = latitude

t = time

$\kappa = R/c_p \approx \frac{2}{7}$

J = heating per unit mass

a = radius of earth

H = constant scale height

We will now follow the spirit of the development in Holton [1975], although some normaliza-

tion factors will differ. Assume the perturbations to consist of longitudinally propagating waves of zonal wavenumber s and frequency σ:

$$\{u, v, \Phi\} = \{\hat{u}, \hat{v}, \hat{\Phi}\} exp[i(s\lambda - \sigma t)] \tag{5}$$

This $(s\lambda - \sigma t)$ form for the phase is chosen so that positive values for σ correspond to eastward propagating waves and negative values to westward propagating waves (i.e., the real part of (5) is $\cos(s\lambda - \sigma t)$ and the crest of the wave occurs where $\lambda = \sigma t/s$). Substituting (5) into (1) - (4) eliminates derivatives with respect to t and λ, permitting consolidation into a single second-order partial differential equation for Φ in z and θ. Separable solutions of the following form exist where $\{\Theta_n\}_{all\ n}$ is a complete orthogonal set:

$$\hat{\Phi} = \sum_n \Theta_n(\theta) G_n(z) \tag{6}$$

$$\hat{J} = \sum_n \Theta_n(\theta) J_n(z) \tag{7}$$

$$\hat{u} = \frac{\sigma}{4\Omega^2 a} \sum_n U_n(\theta) G_n(z) \tag{8}$$

$$\hat{v} = \frac{-i\sigma}{4\Omega^2 a} \sum_n V_n(\theta) G_n(z) \tag{9}$$

where

$$U_n = \frac{1}{(f^2 - \sin^2\theta)} [\frac{s}{\cos\theta} + \frac{\sin\theta}{f} \frac{d}{d\theta}] \Theta_n \tag{10}$$

$$V_n = \frac{1}{(f^2 - \sin^2\theta)} [\frac{s\tan\theta}{f} + \frac{d}{d\theta}] \Theta_n \tag{11}$$

The condition for separability is as follows:

$$i\sigma[\frac{1}{\rho_o}\frac{\partial}{\partial z}(\frac{\rho_o}{N^2})\frac{\partial}{\partial z}G_n] + \frac{1}{\rho_o}\frac{\partial}{\partial z}(\frac{\rho_o \kappa J_n}{HN^2}) = -\frac{i\sigma}{gh_n}G_n \tag{12}$$

where h_n arises as the separation constant. Defining $G'_n = G_n \rho^{1/2} N^{-1}$, assuming an isothermal atmosphere for which $N^2 = \frac{\kappa g}{H}$ where H = constant = 7.5 km (corresponding to $T_o = 256K$), and letting $x = z/H$, results in the *vertical structure equation* (for an isothermal atmosphere):

$$\frac{d^2 G'_n}{dx^2} + [\frac{\kappa H}{h_n} - \frac{1}{4}]G'_n = -\frac{\rho_o^{-1/2}}{i\sigma N}\frac{d}{dx}(\rho_o \kappa J_n) \tag{13}$$

The θ-dependent part of the solution is embodied in *Laplace's tidal equation* [Laplace, 1799, 1825]:

$$\frac{d}{d\mu}[\frac{(1-\mu^2)}{(f^2-\mu^2)}\frac{d\Theta_n}{d\mu}] - \frac{1}{f^2-\mu^2}[-\frac{s}{f}\frac{(f^2+\mu^2)}{(f^2-\mu^2)} + \frac{s^2}{1-\mu^2}]\Theta_n + \epsilon\Theta_n = 0 \tag{14}$$

where $\mu = \sin\theta$ and $\epsilon_n = (2\Omega a)^2/gh_n$. We will now examine solutions to the vertical structure equation and Laplace's tidal equation. Note that they are linked through h_n, which is referred to as the "equivalent depth". This nomenclature originates from the first appearance of equation (14) in connection with the ocean tide problem where h is the ocean depth [Laplace, 1799, 1825; Taylor, 1936].

2.2 Vertical Structure Equation: Forced and Free Solutions

Rewriting (13) as follows

$$\frac{d^2 G'_n}{dx^2} + \alpha^2 G'_n = F(x) \tag{15}$$

where $\alpha^2 = \frac{\kappa H}{h_n} - \frac{1}{4}$, the form of the solution is

$$G'_n \sim Ae^{i\alpha x} + Be^{-i\alpha x} \tag{16}$$

Now we will examine the cases where $F(x) \neq 0$ ("forced" solution) and where $F(x) = 0$ ("free" solution). When $F(x) \neq 0$ there are two possibilities. If $h_n < 0$ or $h_n > 4\kappa H$, then $\alpha^2 < 0$ and

$$G_n' \sim e^{-|\alpha|x} \tag{17}$$

above the source region for a bounded solution. In this case the solutions are referred to as "evanescent" or "trapped" since the wave oscillations are more or less confined to the region of excitation. If $0 < h_n < 4\kappa H$, then $\alpha^2 > 0$ and a "radiation condition" ($C_{gz} > 0$) at $x = \infty$ implies

$$G_n' \sim e^{\pm i|\alpha|x} \tag{18}$$

where (+ , -) corresponds to (westward , eastward) propagating waves (see Section 2.4). This is the so-called propagating solution, where the wave propagates away from the source region.

When $F(x) = 0$ the only nontrivial solution satisfying boundedness and $w = 0$ at $z = 0$ is:

$$G_n' \sim e^{(\kappa - \frac{1}{2})x} \tag{19}$$

and

$$h_n = \frac{H}{1 - \kappa} \tag{20}$$

where $h_n = 10.5$ km for H = 7.5 km. This free (unforced) solution corresponds to a resonant response of the atmosphere. Note that the above solution implies

$$u \sim e^{\kappa x} \tag{21}$$

corresponding to energy decay away from the surface (ρu^2) while horizontal velocity and other wave fields increase exponentially (by a factor of 40 from the surface to 100 km). These waves are sometimes called "Lamb" or "edge" waves. Furthermore, for $h_n = 10.5$ km α^2 is negative, implying no vertical flux of energy out of the atmosphere ($w = 0$) and no phase change with height. Without dissipation, such free oscillations would continue indefinitely without forcing [Lindzen and Blake, 1972].

2.3 Laplace's Tidal Equation: Nomenclature and Classification of Wave Modes

Laplace's tidal equation is often written as follows to emphasize the explicit dependences on s, σ, and ϵ_n:

$$F_{s,\sigma}(\Theta_n^{s,\sigma}) = \epsilon_n^{s,\sigma}\Theta_n^{s,\sigma} \tag{22}$$

For each choice of s and σ, there exists a set of ϵ_n and Θ_n which satisfy (22). The ϵ_n^s and σ are generally related parametrically for a given s in diagrams like the ones comprising Figure 4 for s=1. (Diagrams for s=2 and s=3 are very similar to Figure 4, and are not shown here to conserve space.) Two families of curves are evident for either eastward-propagating ($\frac{\sigma}{s} > 0$) or westward-propagating ($\frac{\sigma}{s} < 0$) solutions. These are sometimes referred to as "Class I" or "Solutions of the First Kind" and "Class II" or "Solutions of the Second Kind" A more common usage is to refer to the first class as "gravity modes" and the second class as "Rossby" , "rotational" or "planetary wave" modes. There are energy partitionings and other properties which differ between these two classes of solutions [Longuet-Higgins, 1968], but we will no concern ourselves with these issues. The remainder of this tutorial will mainly use the terms "gravity" and "Rossby" to distinguish the wave types.

We note from Figure 4 some general features and properties. For instance, gravity (Class I) modes always have $\epsilon_n > 0$, whether they are westward-propagating or eastward-

propagating. On the other hand, Rossby (Class II) modes only possess $\epsilon_n > 0$ for westward-propagating waves; in all other cases the Rossby modes have $\epsilon_n < 0$. From the expression for α^2 in (15), for negative or sufficiently small ϵ_n (or large h_n) the vertical structures are "trapped" or "evanescent", whereas for ϵ_n greater than about 100 solutions are propagating with vertical wavelengths less than 100 km. Note that the (1,-1) mode in Figure 4 belongs to the Rossby mode class for $\epsilon_n^1 < 10$ but joins the Gravity mode family of curves for $\epsilon_n^1 > 10$. This is the so-called mixed Rossby-gravity wave. This mode exists for higher wavenumbers as well. The eastward-propagating ($\sigma > 0$) gravity modes in Figure 4 are referred to as Kelvin waves.

The collection of all Θ_n are the eigenfunctions of Laplace's tidal equation, and are called Hough functions in honor of the individual who pioneered in their numerical computation [Hough, 1897, 1898]. Either the ϵ_n or the h_n (where $\epsilon_n = \frac{4\Omega^2 a^2}{g h_n} \approx \frac{88km}{h_n}$) are referred to as eigenvalues of the system. Each eigenfunction/eigenvalue pair constitutes a "mode". A common nomenclature in identifying modes is to explicitly express s, the zonal wavenumber, and n, the meridional index (so-named since it provides information on the number of latitudinal nodes and symmetry characterizing Θ_n). It is common therefore to refer to a particular mode as the Θ_n^s mode or just the (s,n) mode, and to add some information on wave period, as in the "(1,-2) diurnal tide" The (1,-2) diurnal mode might also be referred to as the "first symmetric trapped diurnal tide" and the "(1,1) mode" as the "first symmetric propagating diurnal tide" Note also from Figure 4 that the (1,-2) mode can assume other periods; at the free mode value of $\epsilon_n = 8.4$ ($h_n = 10.5$ km) for a 256 K isothermal atmosphere, the (1,-2) mode would represent the "5-day wave" ($\frac{\sigma}{\Omega} \approx$ -0.20).

The above experience in locating the "5-day wave" alludes to two possible ways in which diagrams like Figure 4 can be utilized. For forced modes we generally know the frequency of forcing, σ; by drawing a vertical line at $\frac{\sigma}{\Omega}$ on Figure 4, the points of intersection define the ϵ_n^1 values corresponding to the modes which comprise the response at that frequency. This provides information on the vertical structure of the forced response. The

points of intersection corresponding to the diurnal tide ($\frac{\sigma}{\Omega}$ = - 1.0) are indicated in Figure 4. We see that the response consists of a mixture of trapped ((1,-1), (1,-2) .....) and propagating ((1,1), (1,2), ...) modes, the latter with vertical wavelengths between 15 and 50 km. This means that some localized heating in the lower atmosphere will result in (a) several modes which propagate to higher levels; and (b) a response partially contained at the levels of excitation. (The e-folding distance of the latter will depend on the value of ϵ_n). The degree to which the response falls into either of these categories is determined by how well the horizontal and vertical structures of these modes matches that of the forcing. Examination of the analog of Figure 4 for s=2 (not shown here) would show the semidiurnal response ($\frac{\sigma}{\Omega}$ = -2.0) to consist only of propagating modes ($\epsilon_n > 0$); Rossby modes at frequencies higher than 2Ω do not exist.

For free (unforced) modes, we know that $\epsilon_n = 8.4$ for an isothermal atmosphere at 256 K. In Figure 4 the horizontal line defines the free or normal modes that exist for s=1. Looking down from the points of intersection (labelled "NM"), we can then infer the frequencies or periods of the normal modes. For s=1, these occur approximately at periods of 28 hours, 5 days, 8 days, and 12 days, and so on. According to our present nomenclature, we may refer to the last three of these, respectively, as the (1,-2), (1,-3), and (1,-4) westward-propagating Rossby modes of zonal wavenumber one. The 28-hour mode is a mixed Rossby-gravity mode, and is designated (1,-1). At periods of order 1 day or less, this mode behaves like a Rossby mode; at longer periods, it is gravity-like (i.e., propagating) in its character. Similarly, if one examines the s=3 family of curves (not shown here), we would find that the mixed Rossby-gravity normal mode for s=3 occurs close to $\frac{\sigma}{\Omega}$ = -.5, corresponding to the "2-day wave".

Table 1 lists some of the more common westward-propagating modes and their nomenclatures, with approximate values of h_n and the corresponding vertical scale in an isothermal atmosphere calculated from

$$\lambda_z = \frac{2\pi}{\alpha} = \frac{2\pi H}{\sqrt{\frac{\kappa H}{h_n} - \frac{1}{4}}} \tag{23}$$

The present nomenclature is consistent with that of Volland [1988] and Chapman and Lindzen [1970]. In this nomenclature a mode is symmetric about the equator if (n+s) is even (odd) and antisymmetric if (n+s) is odd (even) for gravity (Rossby) solutions. The mixed Rossby-gravity modes obey the Rossby mode symmetry conditions. For symmetric modes Θ_n (and hence all variables δp, $\delta \rho$, δT, w, and u) are mirror images with respect to the equator, whereas v is antisymmetric; for antisymmetric modes v is symmetric and the other variables change sign at the equatorial node. Another commonly used nomenclature used for planetary waves is due to Longuet-Higgins [1968], and is based on the value of $(|n| - s)$. This notation is also provided in Table 1.

Figure 5 illustrates the Θ_n for the first three westward propagating free Rossby modes for s=1. Note that these are global scale modes with maximum amplitudes at middle and high latitudes. Figures 6 and 7 illustrate the corresponding Θ_n for the diurnal and semidiurnal tides, respectively. Also shown are the velocity expansion functions U_n and V_n defined by equations (10) and (11). For the diurnal tide, note the relative concentration of Θ_n, U_n, and V_n at low latitudes for the propagating ($h_n > 0$) modes and high latitudes for the trapped ($h_n < 0$) modes. The propagating modes are also more oscillatory in character. The semidiurnal wind expansion functions, on the other hand, tend to maximize at middle to high latitudes, increasingly so as the meridional index of the mode increases. This provides the first hint of why wind observations around the mesopause should appear predominantly semidiurnal in character at middle to high latitudes, and more diurnal in character at low latitudes (cf. Figure 1).

Table 1

Nomenclatures and other data for various common westward-propagating waves in the middle and upper atmosphere. The column (s, n) indicates the nomenclature used in the present work, and in Volland [1988] and Chapman and Lindzen [1970]. The column $(s, |n| - s)$ indicates the nomenclature, generally restricted to planetary-wave usage, used by Salby [1981a,b; 1984] and Longuet-Higgins [1968]. Also provided are the equivalent depth for each mode [Chapman and Lindzen, 1970], h_n, propagating-mode vertical wavelengths λ_z for an isothermal atmosphere at 256 K, and further descriptors pertaining to the wave. Note that many of the values of λ_z in the real atmosphere vary significantly from the isothermal values given below, especially above and below the mesopuase where the dT/dz term in Equation (26) (cf. Equation (23)) plays an important role.

Wave	(s,n)	$(s, \|n\| - s)$	$h_n(km)$	$\lambda_z(km)$	*Additional Descriptors*
Diurnal tide	(1,1)		0.6909	27.9	Gravity; first symmetric propagating
Diurnal tide	(1,2)		0.2384	15.9	Gravity; first asymmetric propagating
Diurnal tide	(1,3)		0.1203	11.2	Gravity; second symmetric propagating
Diurnal tide	(1,-1)		803.356		Rotational; first asymmetric trapped
Diurnal tide	(1,-2)		-12.2703		Rotational; first symmetric trapped
Diurnal tide	(1,-4)		-1.7581		Rotational; second symmetric trapped
Semidiurnal tide	(2,2)		7.8519	311.	Gravity; first symmetric (propagating)
Semidiurnal tide	(2,3)		3.6665	81.4	Gravity; first asymmetric (propagating)
Semidiurnal tide	(2,4)		2.1098	53.8	Gravity; second symmetric (propagating)
Semidiurnal tide	(2,5)		1.3671	41.0	Gravity; second asymmetric (propagating)
Semidiurnal tide	(2,6)		0.9565	33.4	Gravity; third symmetric (propagating)
5-day wave	(1,-2)	(1,1)	10.5		Rotational; Rossby; first symmetric
10-day wave	(1,-3)	(1,2)	10.5		Rotational; Rossby; first asymmetric
16-day wave	(1,-4)	(1,3)	10.5		Rotational; Rossby; second symmetric
4-day wave	(2,-3)	(2,1)	10.5		Rotational; Rossby; first symmetric
2-day wave	(3,-3)	(3,0)	10.5		Mixed Rossby-Gravity; asymmetric

2.4 Group and Phase Velocity

Let us now return to our "propagating" solution to the vertical structure equation at the beginning of Section 2.2. If $0 < h_n < 4\kappa H$, then $\alpha^2 > 0$ and the form of the solution (16) consists of an upgoing and downgoing wave. Imposition of a "radiation condition" at the top of our domain determines which term in (16) to retain. The radiation condition demands that at sufficiently high altitudes the energy is upgoing, i.e., the vertical group velocity is positive, or $C_{gz} > 0$. To derive this condition, note that since

$$\alpha_n^2 = \frac{\kappa H}{h_n} - \frac{1}{4} = \frac{\kappa H g \epsilon_n}{(2\Omega a)^2} - \frac{1}{4} \tag{24}$$

then

$$C_{gz} = \frac{\partial \sigma}{\partial \alpha} = \pm 2\alpha \frac{\partial \sigma}{\partial \epsilon} / \frac{\partial \alpha^2}{\partial \epsilon} = \pm \alpha \frac{8\Omega^2 a^2}{\kappa g H} \frac{\partial \sigma}{\partial \epsilon} \tag{25}$$

[cf. Andrews et al., 1987, p.164). The choice of sign in front of α must be consistent with that in (18). From Figure 4, we see that $\frac{\partial \sigma}{\partial \epsilon} > 0$ for westward-propagating waves and $\frac{\partial \sigma}{\partial \epsilon} < 0$ for eastward-propagating waves. Therefore, to maintain $C_{gz} > 0$, in (25) we must choose $+\alpha$ for westward propagating waves and $-\alpha$ for eastward propagating waves.

Now, let us see what this implies in terms of phase progression in height and longitude. Our solution for propagating modes is of the form

$$e^{i(s\lambda \pm \alpha z - \sigma t)}$$

The equation $s\lambda \pm \alpha x - \sigma t = K$ defines the line of constant phase, e.g., the crest of the oscillation if $K = 0$. At a fixed λ, $\pm \alpha x - \sigma t = K'$. Therefore, for either westward propagating ($\sigma < 0, +\alpha$) or eastward propagating ($\sigma > 0, -\alpha$) waves we have $x = \frac{\sigma}{\pm \alpha} t + K''$, i.e., downward phase progression as time increases. (We see now why the downward phase progressions characterizing Figure 1 are consistent with a wave source at lower heights, i.e., O_3 and H_2O insolation absorption, and upward propagation through the mesopause.)

Continuing, for a fixed t we have $s\lambda \pm \alpha x = K'$ or $x = -\frac{s}{\alpha}\lambda + K''$ ($x = +\frac{s}{\alpha}\lambda + K''$) implying westward (eastward) phase tilt for westward (eastward) propagating waves. Therefore, westward (eastward) phase tilt for westward- (eastward-) propagating waves is consistent with downward phase progression and upward energy propagation. These are important features to look for in observational data to verify theoretical interpretations.

2.5 Effects of Temperature Structure, Dissipation, and Mean Winds

In Section 2.3 we showed that free oscillations exist in an isothermal, dissipationless atmosphere. For $T_o = 256$ K, h_n and ϵ_n assume values of 10.5 km and 8.4, respectively. In Section 2.2 we were able to find the points of intersection corresponding to $\epsilon_n = 8.4$, and to infer the periods and horizontal structures of the various free modes. Presently, we will discuss in simple terms how the additional complexities of vertical temperature structure, mean zonal winds, and dissipation modify our concepts about free atmospheric oscillations. In Section 4 we will examine the effects of more complicated distributions of winds and temperatures that necessitate comprehensive numerical treatment of the problem.

In a non-isothermal atmosphere, the definition of α^2 in (15) is as follows:

$$\alpha^2 = \frac{\kappa H + dH/dx}{h_n} - \frac{1}{4} \tag{26}$$

Above $\approx$ 90 km $\alpha^2 > 0$, implying propagating solutions, energy leakage into the thermosphere, and a finite time for the oscillations in the absence of continual forcing. A true resonance (infinite response) no longer exists. Lindzen and Blake [1972] assumed a mean distribution of temperature with height, solved (15) and (26) subject to a specification of tropospheric heating, and examined the response (surface perturbation pressure) as a function of the equivalent depth (h_n in (26)). Their result is shown in Figure 8a, and illustrates a sharp but finite maximum at h = 9.95 km. Their solutions also exhibited amplitude growth and phase tilt with height above 90 km, and nonzero vertical velocities when T_o varies with height.

Lindzen and Blake [1972] also examined the influences of eddy and molecular dissipation and surface friction on the Lamb modes. In this case the response is dependent on wave period. Figure 8b illustrates the analog to Figure 8a, except that dissipation is taken into account. Figure 8c illustrates the additional effects of including surface friction. We see that the effects of dissipation and surface friction are to reduce the magnitude and significantly broaden the response, with increasing effects as the period becomes longer. It is also evident that surface friction dominates over internal dissipation, and is therefore the determining factor in limiting the "lifetime" of free modes. Lindzen and Blake estimate lifetimes on the order of 10 to 100 wave cycles for periods between 24 hours and 2 hours, respectively.

Salby [1979, 1980] examined the resonance characteristics of Lamb modes in the presence of vertical temperature structure and dissipation, with emphasis on the longer-period 'Lamb' waves (2 to 20 days). His results for the s=1 Rossby-gravity mode are illustrated in Figure 9. He notes the secondary peak occuring near h = 6.4 km, which was discovered by Pekeris [1937]. This secondary peak is due to the stratospheric temperature duct, and was apparently overlooked by Lindzen and Blake who only took their calculations down to h = 8.5 km. This secondary peak disappears in the presence of realistic dissipation [Salby, 1979; see Figure 9]. In honor of the original discoverer, Platzman [1988] has suggested referring to this as the 'Pekeris' mode.

Lindzen and Blake [1972] did not find any noticeable effects on amplitude and phase structures due to dissipation below 100 km for Lamb periods < 24 hours. However, for the longer-period modes examined by Salby, increased amplitude reduction and phase tilt with height accompany an increase in wave period (see Figure 10). Figure 10 also implies that phase tilt with height in the real atmosphere is not inconsistent with the concept of a free atmospheric mode. Enhanced vertical leakage of energy should diminish wave lifetimes, but the dominant effect remains to be surface friction. Salby's work also suggests free mode lifetimes to be on the order of tens of wave cycles, and also discusses the role of variations in dissipation in reflection of wave modes, particularly when the doppler-shifted

frequency becomes small.

The zero-order effects of non-zero winds can be ascertained quite easily. If we suppose that the troposphere is characterized by a mean eastward wind $\overline{U}\sin\theta$ (effectively a uniform superrotation of the atmosphere), then the σ appearing in our equations

$$\frac{\partial}{\partial t} \rightarrow -i\sigma$$

should be replaced by the Doppler-shifted or intrinsic frequency, σ_D:

$$\frac{\partial}{\partial t} + \frac{\overline{U}}{a}\frac{\partial}{\partial \lambda} \rightarrow -i(\sigma - k\overline{U}) = -i\sigma_D$$

where $k = \frac{s}{a}$. In this case, the horizontal scale in Figure 4 is σ_D/Ω, not σ/Ω. To an observer on the ground, however, the wave frequency would be

$$\sigma_{obs} = \sigma_D + k\overline{U},$$

or equivalently, the observed period is

$$T_{obs} = \frac{2\pi}{|\sigma_D + k\overline{U}|}$$

For the (1,-2), (1,-3), and (1,-4) normal modes for which $\epsilon = 8.4$, we infer from Figure 4 the corresponding normalized frequencies of about -0.2, -0.12, -0.08, or periods of 5, 8.3, and 12.5 days, respectively. If we interpret these to be Doppler-shifted frequencies, then for a nominal value of $\overline{U} = 10$ ms^{-1}, the *observed* periods ought to be about 5.6, 10.2, and 17.1 days. Therefore, we expect the actual atmospheric manifestations of free Rossby modes to be Doppler-shifted to longer periods. This is why we associate, for instance, the observed 2-3 week oscillation referred to as the "quasi 16-day wave" [Madden, 1979] with the (1,-4) Rossby mode possessing an eigenperiod of only 12.5 days.

3. FORCING OF ATMOSPHERIC TIDES

Atmospheric tides represent an obvious example of "forced" atmospheric waves for which we know the wave periods quite well. Lunar tides are of course determined by the period of the moon's *apparent* rotation around the earth. Here we will be mainly concerned with solar or thermally-forced tides, which are excited by the periodic absorption of solar radiation connected with the *apparent* motion of the Sun around the Earth. Figure 11 is a schematic of the main points: Various parts of the solar spectrum are absorbed by tropospheric water vapor (near-IR), stratospheric ozone (UV), and major atmospheric constituents (O_2 and N_2) in the lower thermosphere (Figure 11a). (Note that the region around the mesopause, where most meteor and MF radar measurements provide wind data, cf., Figures 1-3, are in a region of "no excitation" At any given height, the day-night variation of absorbed radiation (and hence heating) gives rise to Fourier components which are integral subharmonics of a solar day: 24 hours, 12 hours, 8 hours, etc.; Figure 11b). Each of these harmonic components (referred to as the diurnal tide, semidiurnal tide, terdiurnal tide, respectively) possess a height-latitude distribution (we are ignoring longitude dependences for the moment). Near the height of maximum heating, the latitudinal distribution for a given harmonic might look something like Figure 11c (i.e., maximum at low latitudes and minimum at the poles, in concert with the solar zenith angle influence).

Now, given that the Θ_n form a complete orthogonal set, we can expand the height-latitude distribution of heating for a given frequency component, $J^\sigma(z,\theta)$ (cf. equation (7)):

$$J^\sigma(z,\theta) = \sum \Theta_n(\theta) J_n(z)$$

Each "mode" defined by its eigenfunction-eigenvalue pair (Θ_n, h_n) now possesses its own vertical profile of heating $J_n(z)$. The vertical structure of each mode is determined by $J_n(z)$, h_n, and the mean thermal structure of the atmosphere vis-a-vis Equations (15) and (6).

Typical examples of $J_n(z)$ for diurnal and semidiurnal tides are provided in Figure 12 [Forbes and Garrett, 1978]. Note that most of the heating goes into the (1,-2) mode for the diurnal tide, and into the (2,2) mode for the semidurnal tide, as the Θ_n for these modes (cf. Figures 6 and 7) most closely correspond with the latitudinal distribution of heating (cf. Figure 11b).

4. NUMERICAL MODEL RESULTS

4.1 Atmospheric Tides

In Section 2 we discussed the eigenfunction-eigenvalue problem corresponding to forced and free atmospheric oscillations in an isothermal, dissipationless atmosphere. By definition "separability" existed, so that each mode possessed its own vertical structure. (Indeed, use of the term "mode" implies separability). Separability of height and latitude dependences also exists in a non-isothermal atmosphere, and additionally for special treatments of height-dependent dissipation [Lindzen and McKenzie, 1967; Lindzen, 1970]. However, in the joint presence of latitude-dependent rotation and vertical diffusion of heat and momentum, or in the presence of latitude dependent mean winds, the equations for an oscillation with specified frequency and zonal wavenumber are nonseparable. First of all, this necessitates a numerical approach to the problem; secondly, strictly speaking, this precludes reference to "modes" particularly in the mesosphere and lower thermosphere. However, it is commonplace to use modal terminology nontheless, as many observed features of prominent oscillations exhibit characteristics very similar to what would be expected on the basis of "classical" theory. In fact, it is commonplace to decompose the thermal forcing in numerical models into Hough modes (as in Figure 12), even though the solution is nonseparable; and in fact, the solutions are sometimes decomposed into Hough modes to facilitate interpretation of the results. We will now breifly review some of these numerical models.

Forbes and Garrett [1979] review basically two types of numerical models which take

into account dissipation, mean winds, and other processes in simulations of middle and upper atmosphere tides. The first genre neglect eddy and molecular dissipation, but include mean winds and meridional temperature gradients, Newtonian cooling, and perhaps a Rayleigh friction (linear damping) term to filter out small-scale noise or to facilitate application of upper boundary conditions. Dispensing with diffusion allows one to derive a single second-order partial differential equation in height and latitude for the perturbation geopotential [Lindzen and Hong, 1974; Aso et al., 1981; Walterscheid et al., 1979a,b; 1980; Vial, 1987; Forbes and Vial, 1989]. In the context of the solution of these nonseparable equations, the terminology of "mode coupling" has arisen. This refers to the generation of tidal modes (determined through an orthogonal expansion of the calculated response) which are not forced directly by thermal excitation, but which arise because of the non-separability of the governing equation. For instance, if only the (2,2) mode is excited in these models, the response at say 90 km consists of many modes ((2,2), (2,3) , ...) due to the "distorting" effects of the mean wind distribution. In the above models the (2,4) mode appears to receive about equal contributions from direct thermal forcing and mode coupling via the (2,2)-mean wind interactions which tend to add in phase. On the other hand, for the (2,3) mode the effect of mode coupling is to interfere with the directly forced component and thereby reduce the (2,3) response above the level of ozone heating. In the case of (2,5), excitation appears to arise almost exclusively due to direct thermal forcing (mode coupling is weak). More recent studies by Forbes and Hagan [1987] and Vial [1986] address the diurnal tide, and utilize a Rayleigh friction (linear damping) term to parameterize turbulent diffusion of momentum. For the dominant diurnal propagating (1,1) mode, latitudinal broadening (or leakage to high latitudes) due to dissipation near 90 km can be viewed as a coupling into the trapped or evanescent (1,-2) mode, whereas the asymmetries in the modified modal shape induced by the global mean wind distribution (particularly around solstice) can be interpreted as a coupling into the (1,2) and (1,-1) asymmetric modes.

At the next hierarchal level of modeling pertaining to atmospheric tides, Forbes [1982

a,b] includes eddy and molecular diffusion of momentum and heat so as to properly address the structural modification of tides in the 80 - 150 km region and their penetration to higher altitudes. This requires numerical solution of the four coupled partial differential equations in the three velocity components and temperature, as opposed to a single equation for the geopotential as in the above studies. Forbes [1982 a,b] provides explicit simulations from the surface to 400 km for the solar diurnal, solar semidiurnal, and lunar semidiurnal tides due to realistic thermal and gravitational forcing, as well as normalized thermospheric extensions of solar semidiurnal modes above 80 km for use in the fitting, extrapolation and interpolation of observational data [Forbes and Hagan, 1982].

Illustrations of amplitude and phase vertical structures for the solar semidiurnal and diurnal tides from the Forbes [1982 a,b] model are shown in Figures 13 and 14, respectively. In Figure 13, note the relatively long vertical wavelength characterizing the response below 50 km; this is consistent with most of the heating going into the long-wavelength (2,2) mode (Figure 12; Table 1); above about 50 km, the wavelength decreases, due to the increased presence of short-wavelength modes induced by "mode coupling" due to the strong mesospheric jets. The region between 70 and 90 km is a region of evanescence for the (2,2) mode, due to the combined effects of its large h_n and the negative temperature gradient (cf. equations (15) and (6)). However, in this region the higher-order modes are growing exponentially with height, and soon begin to dominate the solution in the lower thermosphere. However, as molecular viscosity begins to dominate in the 120 - 150 km region, these shorter vertical wavelength modes (cf. Table 1) are more susceptible to dissipation, and the longer wavelength modes begin to dominate at higher altitudes. In the upper thermosphere, molecular diffusion of heat and momentum are so efficient that it is difficult to maintain vertical shears in the wind and temperature fields, and the tidal fields asymptote to constant values above about 200 km.

The situation is similar for the diurnal tide, illustrated in Figure 14. Note that at high latitudes (60° in Figure 14) the phase is more or less constant with height, consistent with the dominance of trapped modes whose maxima are at high latitudes (cf. Figure 6).

At low latitudes the solution is dominated by the (1,1) mode, with a vertical wavelength of order 30 km (cf. Table 1).

At this point we should comment on the characteristics noted in reference to Figure 1 in Section 1. In Section 2.4 the downward phase progression with height was shown to be consistent with a positive (upward) group velocity, consistent with the excitation sources being located somewhere below 80 km. At high latitudes, the tidal fields near the mesopause are dominated by the semidiurnal propagating modes, particularly higher order modes than (2,2); since there is relatively little in-situ heating, the diurnal tide is weak at latitudes greater than about 40°; furthermore, the higher-order semidiurnal tides are growing exponentially with height in this regime where the (2,2) mode is quasi-evanescent. This accounts for the predominance of the semidiurnal tides at Saskatoon in Figure 1. At Townsville (19°S), much closer to the equator, the propagating semidiurnal tides are relatively small, and the diurnal tide enjoys its maximum amplitudes (cf. Figure 6).

4.2 Planetary Waves

Although the above mode coupling effects are important in the context of atmospheric tides, the tidal wave phase speeds are generally large compared to the mean flow speed U; the resulting effects do not represent *drastic* consequences. In effect, these "fast" waves do not "see" the relatively slow background flow. However, as the wave periods increase from 2 to 20 days for planetary (Rossby) waves, the phase speeds get smaller and the effects of mean winds assume much greater importance. The above arguments can be made more quantitative by noting the Doppler-shifting effects of mean winds that appear when assuming solutions of the form $e^{i(s\lambda-\sigma t)}$:

$$\frac{\partial}{\partial t} + \frac{\overline{U}}{a\sin\theta}\frac{\partial}{\partial \lambda} \rightarrow ik(-C_{ph} + \overline{U})$$

where $k = \frac{s}{a\sin\theta}$ and the zonal phase speed is $C_{ph} = \frac{\sigma}{k}$. For the migrating tides $\sigma = s\Omega$, so that $C_{ph} = \Omega a \sin\theta$ or about 464 ms^{-1} at the equator and 232 ms^{-1} at 60° latitude. If T is the period in days, then for the westward propagating planetary waves,

$$C_{ph} = -\frac{\Omega a \sin\theta}{sT}$$

and the above tidal phase speeds are reduced by the factor sT. For the s=1 10-day wave $C_{ph} \approx 23$ ms^{-1} at 60° latitude, and for the s=3 2-day wave $C_{ph} \approx 39$ ms^{-1}. In either case, and for other planetary waves as well, summer easterlies of order -20 to -60 ms^{-1} can obviously have drastic effects on the propagation of planetary waves. When the condition $\sigma_D = -C_{ph} + \overline{U} = 0$ is satisfied, we refer to this as a critical line, and anticipate that this must imply drastic effects (N.B. for stationary planetary waves $C_{ph} = 0$, and this condition reduces to the zero wind line). Moreover, when σ_D becomes small we intuitively expect the wave to be more sensitive to dissipative processes. Below, we will examine the role of zonal mean winds in greater detail.

Salby [1982 a,b] has utilized the first genre of model described above to investigate the behavior of planetary waves in the presence of realistic background winds. In this work he forced the lower boundary with a constant vertical velocity with respect to latitude (with a change of sign at the equator for asymmetric forcing), and examined the response as a function of frequency, with the zonal wavenumber and background wind configuration fixed. An example of his results for s=1 westward propagating modes is illustrated in Figure 15. Note that the response is very structured, and differs considerably between typical equinoctial and solsticial conditions. These results reflect the extreme sensitivity of the planetary wave response to the background wind field. Note, however, that the responses tend to maximize near periods of 5, 9, and 16 days. As Salby shows, the tropospheric and lower stratospheric responses near these periods are structurally similar (i.e., latitude dependence of amplitude and phase) to what we would expect on the basis of "classical theory" presented in Section 2. Therefore, it appears that even in realistic wind configurations that it is valid to speak in terms of a resonant response of the atmosphere, and to associate these responses with the free Rossby modes of Laplace's tidal equation. However, above the lower stratosphere, the atmospheric response is further complicated

by high wind speeds and shears. We will now briefly discuss some of these effects.

Dickinson [1968] has performed an analytic investigation of the vertical propagation of stationary planetary waves through a background wind field consisting of significant vertical and horizontal shears. This theory is applicable to the long-period oscillations investigated here, and provides a framework for interpreting the results. Dickinson's work represents an extension of Charney and Drazin [1961], who limit their analysis to a mean zonal wind independent of latitude with constant Coriolis parameter. Charney and Drazin conclude that vertical propagation of stationary planetary waves is only possible in westerly wind regimes, when the westerly wind speed is below some upper limit (sometimes referred to as the "Charney-Drazin critical speed"). The basic idea of Dickinsons's work can be extended to traveling planetary waves if we simply replace "westerly wind" ($\overline{U} > 0$) with "westerly wind with respect to the wave" ($(\overline{U} - C_{ph}) > 0$). The main conceptual results of Dickinson [1968] are summarized in his Figure 1, which is reproduced here as Figure 16. Assuming winter solstice conditions and a mid-latitude source of wave energy, vertical propagation of planetary waves is affected as follows. At middle latitudes, the westerly jet is sufficiently strong to preclude efficient propagation above the stratopause. Poleward of the westerly jet, a wave guide is formed which traps waves between the strong westerlies and the geometric pole; Dickinson refers to this as the *polar cap wave guide.* This wave guide provides a ducting channel through which planetary waves can penetrate to the mesosphere and lower thermosphere. (A similar ducting channel can in principle be realized between two regions of high westerly wind separated by weak westerlies). Planetary wave disturbances can also be diffracted into an *equatorial wave guide* formed between the westerly jet of the winter hemisphere and the zero-wind line (or critical line in the case of traveling waves) transition to stratospheric summer easterlies. Dickinson's analysis indicates the planetary disturbances would be absorbed rather than reflected along such zero-wind lines, providing an impediment to significant vertical penetration (i.e., to the mesopause). Dickinson therefore suggests that whatever stationary (and therefore long-period) planetary wave disturbances might be realized at the equatorial mesopause would

probably originate from leakage connected with the polar wave guide. It seems reasonable to assume, however, that the degree of attenuation is dependent on the strength of the westerly jet, and the separation distance between the jet and the zero-wind (or critical) line.

A numerical simulation [Salby, 1981c] of the 2-day wave under Northern Hemisphere winter solstice conditions is presented in Figure 17. This is a case of 'moderate' mean wind effects, i.e., not so extreme as the s=1 10-day and 16-day waves. Nevertheless, the tendency for exclusion of the solution from the strong winter westerly and summer easterly jets is evident. In this case the equatorial waveguide is very broad (wide separation between the critical line in the summer Hemisphere and the winter jet maximum). There is also a tendency for the wave maxima to shift to the summer Hemisphere, i.e., to the region of weak westerlies with respect to the wave. Note that the equatorial amplitudes of meridional wind at 35°S are of the same order ($\approx 20 - 30 \mathrm{ms}^{-1}$) as the episodically large 2-day wave amplitudes observed during local summer over Adelaide, S. Australia (Figure 3). Therefore, Figure 17 provides some measure of the true height/latitude temperature and meridional wind distributions for the episodically large 2-day wave.

5. CONCLUDING REMARKS AND OUTLOOK FOR THE FUTURE

This tutorial has sought to expose the non-dynamicist to the fundamental theory, observational evidence, and numerical modeling results pertaining to tides and planetary waves in the mesosphere and lower thermosphere. At this point, there remains much to be done. While radars are capable of providing long time series and therefore identifying the presence of planetary wave periodicities, they are distributed too sparsely to provide adequate information on zonal wavenumbers. On the other hand, satellites are now capable of providing good spatial coverage with marginally useful temporal information. Moreover, the region between 100 and 150 km is practically devoid of any measurements capable of delineating planetary waves. This combination of capabilities and circumstances represents an ideal situation for joint ground-based/satellite observations of the mesosphere/lower

thermosphere (MLT), a task promised to be accomplished by the NASA TIMED Mission.

There is also considerable room for theoretical and numerical modeling advances. The question of nonmigrating (i.e., longitude-dependent) diurnal tides needs to be addressed, and the work of Forbes and Groves [1987] improved upon with greater attention to various tropospheric excitation sources. The pioneering work of Salby [1981a,b,c] needs to be extended, particularly with regard to inclusion of more realistic mean wind distributions and dissipative processes, both of which are essential to understanding the propagation characteristics of planetary waves in the mesosphere and lower thermosphere. The possible in-situ generation of Rossby-like modes in the MLT regime, possibly due to solar radiation or joule heating variations, or the periodic filtering of gravity waves originating in the lower atmosphere and depositing heat and momentum in the upper atmosphere, warrant investigation. Some initial work on gravity-type normal modes of the thermosphere has been accomplished by Larsen and Mikkelesen [1987], but no work has been done on possible Rossby-like normal modes of the thermospheric regime.

As a potential influence of planetary waves on the MLT region, even when they may not penetrate beyond the mesosphere, consider Figure 18. This is a plot of power spectral densities constructed from daily values of the *semidiurnal tidal amplitude* derived from wind observations near 95 km over Obninsk, Russia, during January through February, 1979 (cf. Figure 2). We see that the semidiurnal tide is modulated at periods near 10 days and 20 days, possible due to interactions with mean winds of these periodicities in the mesosphere. The modulations are significant; the 10-day modulation amounts to about ± 7 ms^{-1} about a mean value of ≈ 20 ms^{-1} in the semidiurnal wind amplitude.

Heretofore, studies of tides and planetary waves have considered these wave components to be linearly independent. Besides improving on our modeling and experimental capabilities in this direction, we must now pursue nonlinear interactions between these wave components [cf. Teitelbaum and Vial, 1991], and with the mean dynamics, thermodynamics, and compositional state of the MLT region. The data in Figure 18 demonstrate the

potential influence of planetary waves on the day-to-day variability of atmospheric tides, and underscores the importance of continuous wind and temperature observations. New methods of data analysis must also be explored, such as bispectral estimation which may provide greater insight into the interactions between waves. Finally, considerable progress will not be made until a combined ground-based and satellite-based effort is launched, hopefully in connection with the TIMED mission, to provide the necessary space-time coverage to disentangle the wavenumber/frequency spectra of large-scale waves in the MLT regime.

Acknowledgments. The National Center for Atmospheric Research is sponsored by the National Science Foundation. This work was sponsored by Grant ATM-9102200 from the National Science Foundation to Boston University.

REFERENCES

Andrews, D.G., Holton, J.R., and C.B. Leovy, *Middle Atmosphere Dynamics*, Academic Press, New York, 1987, p. 164.

Aso, T., Nonoyama, T., and S. Kato, Numerical simulation of semidiurnal atmospheric tides, *J. Geophys. Res., 86*, 11,388-11,400, 1981.

Cevolani, G., and S.P. Kingsley, Non-linear effects on tidal and planetary waves in the lower thermosphere: preliminary results, *Adv. Space. Res., 12(10)*, 77-80, 1992.

Chapman, S., and R.S. Lindzen, *Atmospheric Tides*, D. Reidel, Hingham, Mass., 1970.

Charney, J.G., and P.G. Drazin, Propagation of planetary-scale disturbances from the lower into the upper atmosphere, *J. Geophys. Res., 66*, 83-109, 1961.

Dickinson, R.E., Planetary Rossby waves propagating vertically through weak westerly wind wave guides, *J. Atmos. Sci., 25*, 984-1002, 1968.

Forbes, J.M., Atmospheric Tides. I. Model description and results for the solar diurnal component, *J. Geophys. Res., 87*, 5222-5240, 1982a.

Forbes, J.M., Atmospheric Tides, II. The solar and lunar semidiurnal components, *J. Geophys. Res., 87*, 5241-5252, 1982b.

Forbes, J.M., and H.B. Garrett, Thermal excitation of atmospheric tides due to insolation absorption by H_2O and O_3, *Geophys. Res. Lett., 5*, 1013-1016, 1978.

Forbes, J.M., and H.B. Garrett, Theoretical studies of atmospheric tides, *Rev. Geophys. Space Phys., 17*, 1951-1981, 1979.

Forbes, J.M., and M.E. Hagan, Thermospheric extensions of the classical expansion functions for semidiurnal tides, *J. Geophys. Res., 87*, 5253-5259, 1982.

Forbes, J.M., and M.E. Hagan, Diurnal propagating tide in the presence of mean winds and dissipation: a numerical investigation, *Planet. Space Sci., 36*, 579-590, 1988.

Forbes, J.M., and F. Vial, Monthly simulations of the solar semidiurnal tide in the mesosphere and lower thermosphere, *J. Atmos. Terr. Phys., 51*, 649-661, 1989.

Harris, T.J., A long-term study of the quasi-two-day wave in the middle atmosphere, *J. Atmos. Terr. Phys.*, in press, 1993.

Holton, J.R., *The Dynamic Meteorology of the Stratosphere and Mesosphere*, Meteor. Monog. 15(37), Amer. Met. Soc., Mass., 1975.

Hough, S.S., On the application of harmonic analysis to the dynamical theory of tides, Part I., On Laplace's 'Oscillations of the First Species', and on the dynamics of ocean currents, *Phil. Trans. Roy. Soc. London, A189*, 201-257, 1897.

Hough, S.S., On the application of harmonic analysis to the dynamical theory of tides, Part II, On the gneral integration of Laplace's dynamical equations, *Phil. Trans. Roy. Soc. London, A191*, 139-185, 1898.

Laplace, P.S., *Mechanique Celeste, 2*, Paris, 294-298, 1799.

Laplace, P.S., *Mechanique Celeste, 5*, Paris, 145-169, 1825.

Larsen, M.F., and I.S. Mikkelsen, The normal modes of the thermosphere, *J. Geophys. Res., 92*, 6023-6043, 1982.

Lindzen, R.S., Internal gravity waves in atmospheres with realistic dissipation and temperature, I. Mathematical development and propagation of waves into the thermosphere, *Geophys. Fl. Dyn., 1*, 303-355, 1970.

Lindzen, R.S., and D. Blake, Lamb waves in the presence of realistic distributions of temperature and dissipation, *J. Geophys. Res., 77*, 2166-2176, 1972.

Lindzen, R.S., and S.-S. Hong, Effects of mean winds and horizontal temperature gradients on solar and lunar tides in the atmosphere, *J. Atmos. Sci., 31*, 1421-1466, 1974.

Lindzen, R.S., and D.J. McKenzie, Tidal theory with Newtonian cooling, *Pageoph., 66*, 90-96, 1967.

Longuet-Higgins, M.S., The eigenfunctions of Laplace's tidal equation over a sphere, *Phil.*

Trans. Roy. Soc. London, A262, 511-607, 1968.

Madden, R.A., Observations of large-scale traveling Rossby waves, *Rev. Geophys. Space Phys., 17*, 1935-1950, 1979.

Pekeris, C.L., Atmospheric Oscillations, *Proc. Roy. Soc. London, A158*, 650-671, 1937.

Platzman, G.W., The atmospheric tide as a continuous spectrum: lunar semidiurnal tide in surface pressure, *Meteorol. Atmos. Phys., 38*, 70-88, 1988.

Pogoreltsev, A.I., and S.A. Sukhanova, Simulation of the global structure of stationary planetary waves in the mesosphere and lower thermosphere, *J. Atmos. Terr. Phys., 55*, 33-40, 1993.

Salby, M.L., On the solution of the homogeneous vertical structure problem for long-period oscillations, *J. Atmos. Sci., 36*, 2350-2359, 1979.

Salby, M.L., The influence of realistic dissipation on planetary normal structures, *J. Atmos. Sci., 37*, 2186-2199, 1980.

Salby, M.L., Rossby normal modes in nonuniform background configurations. Part I: Simple fields, *J. Atmos. Sci., 38*, 1803-1826, 1981a.

Salby, M.L., Rossby normal modes in nonuniform background configurations. Part II: Equinox and solstice conditions, *J. Atmos. Sci., 38*, 1827-1840, 1981b.

Salby, M.L., The 2-day wave in the middle atmosphere: observations and theory, *J. Geophys. Res., 86*, 9654-9660, 1981.

Salby, M.L., Survey of planetary-scale traveling waves: The state of theory and observation, *Rev. Geophys. Space. Phys., 22*, 209-236, 1984.

Taylor, G.I., The oscillations of the atmosphere, *Proc. Roy. Soc. London, A156*, 318-326, 1936.

Teitelbaum, H., and F. Vial, On tidal variability induced by non-linear interaction with planetary waves, *J. Geophys. Res., 96*, 14,169-14,178, 1991.

Vial, F., Numerical simulations of atmospheric tides for solstice conditions, *J. Geophys. Res., 91*, 8955-8969, 1987.

Vincent, R.A., Planetary and gravity waves in the mesosphere and lower thermosphere, *Adv. Space Res., 10*, 93-101, 1990.

Volland, H., *Atmospheric Tidal and Planetary Waves*, Kluwer Academic Publ., Boston, 1988.

Walterscheid, R.L., Traveling planetary waves in the stratosphere, *Pageoph., 118*, 239-265, 1980.

Walterscheid, R.L., and S.V. Venkateswaran, Influence of mean zonal motion and meridional temperature gradients on the solar semidiurnal atmospheric tide: A spectral study. Part 1, Theory, *J. Atmos. Sci., 36*, 1623-1635, 1979a.

Walterscheid, R.L., and S.V. Venkateswaran, Influence of mean zonal motion and meridional temperature gradients on the solar semidiurnal atmospheric tide: A spectral study. Part 2, Numerical results, *J. Atmos. Sci., 36*, 1636-1662, 1979b.

Walterscheid, R.L., DeVore, J.G., and S.V. Venkateswaran, Influence of mean zonal motion and meridional temperature gradients on the solar semidiurnal atmospheric tide: A revised spectral study with improved heating rates, *J. Atmos. Sci., 37*, 455-470, 1980.

Williams, C.R., and S.K. Avery, Analysis of long-period waves using the mesosphere-stratosphere-troposphere radar at Poker Flat, Alaska, *J. Geophys. Res., 97*, 20,855-20,861, 1992.

FIGURE CAPTIONS

Figure 1. Height-local time contours depicting average northward winds during the period March 18-27, 1979, over Townsville, Australia (19°S, 147°E) and Saskatoon, Canada (54°N, 107°W), as measured by the spaced antenna drift method. Data courtesy of Prof. R.A. Vincent and Prof. A.H. Manson.

Figure 2. Power spectrum of daily mean meridional (dashed line) and zonal (solid line) winds observed near the mesopause over Obninsk, Russia (54°N, 38°E) for January through February, 1979. Data courtesy of Dr. Yu.I. Portnyagin.

Figure 3. The amplitude of the quasi two-day wave for January, 1984, through January, 1991, near the mesopause over Adelaide, S. Australia (35°S, 138°E). These amplitudes were determined using a complex demodulation procedure, with an effective bandpass of 44 to 53 hours. Meridional winds are shown in the top panel with the zonal winds below. From Harris [1993].

Figure 4. Eigenvalues ϵ_n^s of wave modes of zonal wavenumber s=1 vs. normalized frequency $\frac{\sigma}{\Omega}$. Waves with positive (negative) frequencies propagate to the east (west). The dots corresponding to $\epsilon_n^1 = 0$ denote the so-called Rossby-Haurwitz waves. The dots corresponding to "NM" refer to the normal modes ($\epsilon_n^1 \approx 8.4$). The vertical series of dots at $\frac{\sigma}{\Omega} = -1.0$ define the ϵ_n^1 for the diurnal tide. The eastward-propagating gravity-type (Class I) modes are the Kelvin Waves. Figure and caption adapted from Volland [1988].

Figure 5. Hough modes corresponding to the first three free Rossby modes of zonal wavenumber one. Adapted from Walterscheid [1980].

Figure 6. Normalized expansion functions for the solar diurnal tide. Top: Hough Function. Middle: Eastward wind expansion function. Bottom: Northward wind expansion function. Solid line, (1,1); dashed, (1,-1); dashed-double dot, (1,2); dashed, (1,-2); dahsed-dot, (1,-4). From Forbes [1982a].

Figure 7. Same as Figure 6, except for the semidiurnal tide. Dashed line, (2,2); solid,

(2,3); dotted, (2,4); dashed-dot, (2,5); dashed-double dot, (2,6). From Forbes [1982b].

Figure 8. Fractional response in surface pressure $|\delta p/p_o|$ as a function of equivalent depth. (a) Without dissipation and without surface friction; (b) With dissipation and without surface friction; (c) with dissipation and with surface friction. From Lindzen and Blake [1972].

Figure 9. Total energy as a function of $\theta = \frac{H}{h_n}$ for the s=1 mixed Rossby-gravity mode, with dissipation (solid line) and without dissipation (dashed line). The secondary peak for the conservative case (dashed line) is due to buoyancy trapping at upper levels [Salby, 1979]. The absence of a secondary peak in the presence of dissipation is due to the reduced energy flux reaching these levels from the surface [Salby, 1980]. Figure and caption adapted from Salby [1980].

Figure 10. Normalized velocity magnitude (top) and phase (bottom) for the lowest order s=1 westward propagating waves in the presence of dissipation. The notation n-m = 0,1,2,3 refers, respectively, to the mixed Rossby-gravity mode, and the "5-day", "10-day", and "16-day" waves. Vertical structures for the true Lamb mode are shown for comparison. From Salby [1980].

Figure 11. Schematic of vertical (left), latitudinal (top) and diurnal (bottom) variations in tidal heating.

Figure 12. Vertical profiles of diurnal (top) and semidiurnal (bottom) heating, $e^{-\frac{x}{2}} J_n$, where $x = -ln(p/p_o)$, due to insolation absorption by ozone and water vapor, corresponding to various solar tidal modes. The units are Joules kg^{-1} sec^{-1}. Adapted from Forbes and Garrett [1978].

Figure 13. Amplitude (left) and phase (right) for solar semidiurnal eastward winds at 0°, ±30°, and ±60° latitude for December solstice conditions. From Forbes [1982b].

Figure 14. Same as Figure 13, except for the solar diurnal tide. From Forbes [1982a].

Figure 15. Simulated atmospheric response as a function of normalized frequency for s=1 westward propagating waves, for typical solstice and equinox background wind

conditions. From Salby [1981b].

Figure 16. Schematic of propagation paths for stationary planetary waves excited in the mid-latitude N. Hemisphere during winter conditions. From Dickinson [1968]. For the traveling planetary waves, the barrier represented here by the zero wind line would be replaced by the frequency-dependent critical line; for periods greater than about 10 days and small zonal wavenumbers, the critical line is close to the zero wind line, and for progressively smaller periods the critical line recedes up into the mesosphere and towards high latitudes.

Figure 17. Simulated meridional wind (ms^{-1}) and temperature (K) as a function of height and latitude for the quasi two-day wave. Typical December solstice conditions are assumed. From Salby [1981c].

Figure 18. Power spectrum of daily amplitudes of semidiurnal meridional wind observed near the mesopause over Obninsk, Russia (54°N, 38°E) for January through February, 1979. Data courtesy of Dr. Yu.I. Portnyagin.

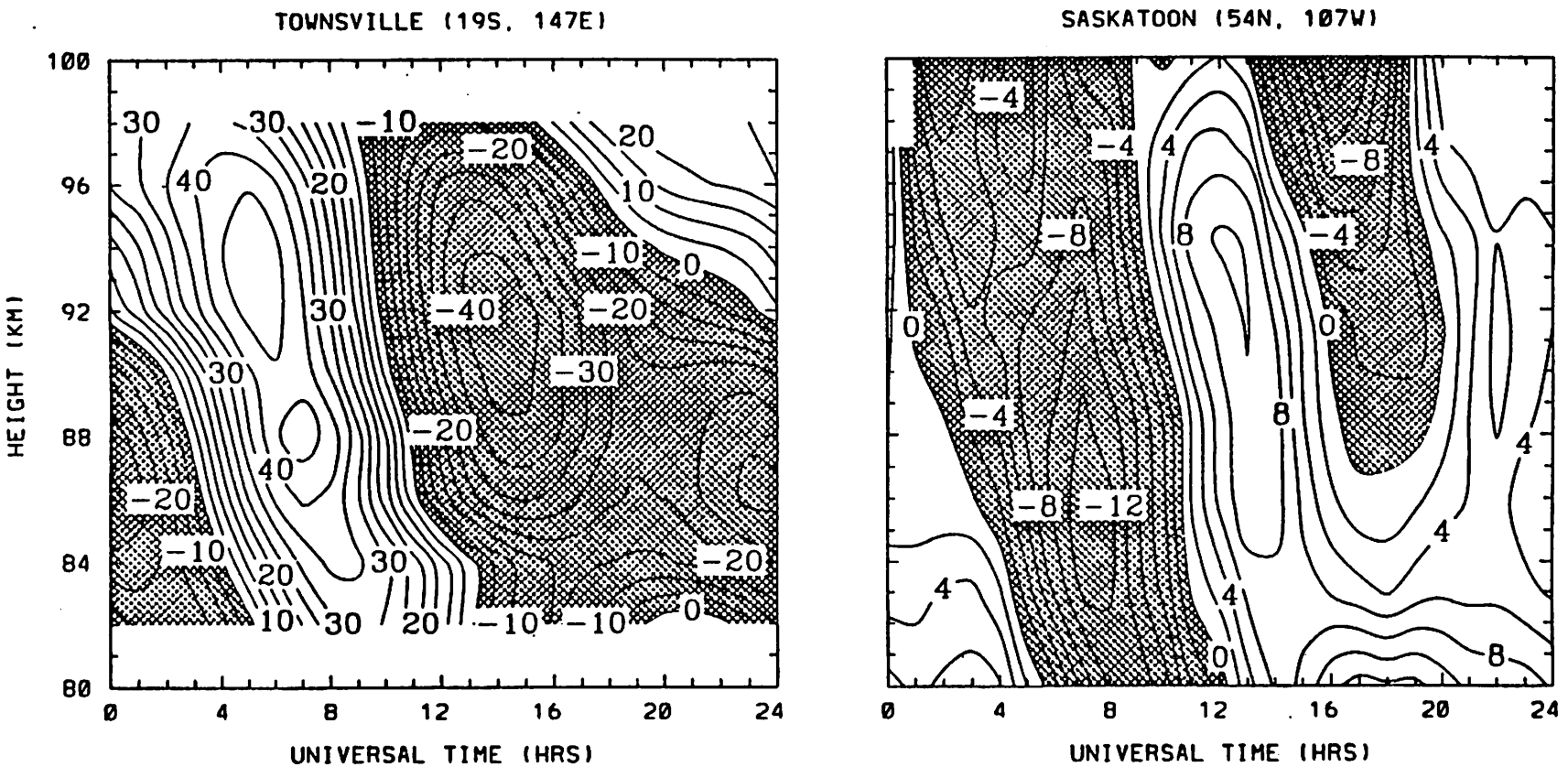
TOWNSVILLE (19S, 147E)
HEIGHT (KM)
100
96
92
88
84
80
0
4
8
12
16
20
24
UNIVERSAL TIME (HRS)
30
-30
-10
-20
20
40
10
-10
0
30
-40
-20
30
-30
-20
40
-20
-10
20
30
-20
10
30
20
-10
-10
0
SASKATOON (54N, 107W)
-4
-4
4
-8
4
-8
8
-4
0
0
-4
8
4
-8
-12
4
4
4
0
8
UNIVERSAL TIME (HRS)

1

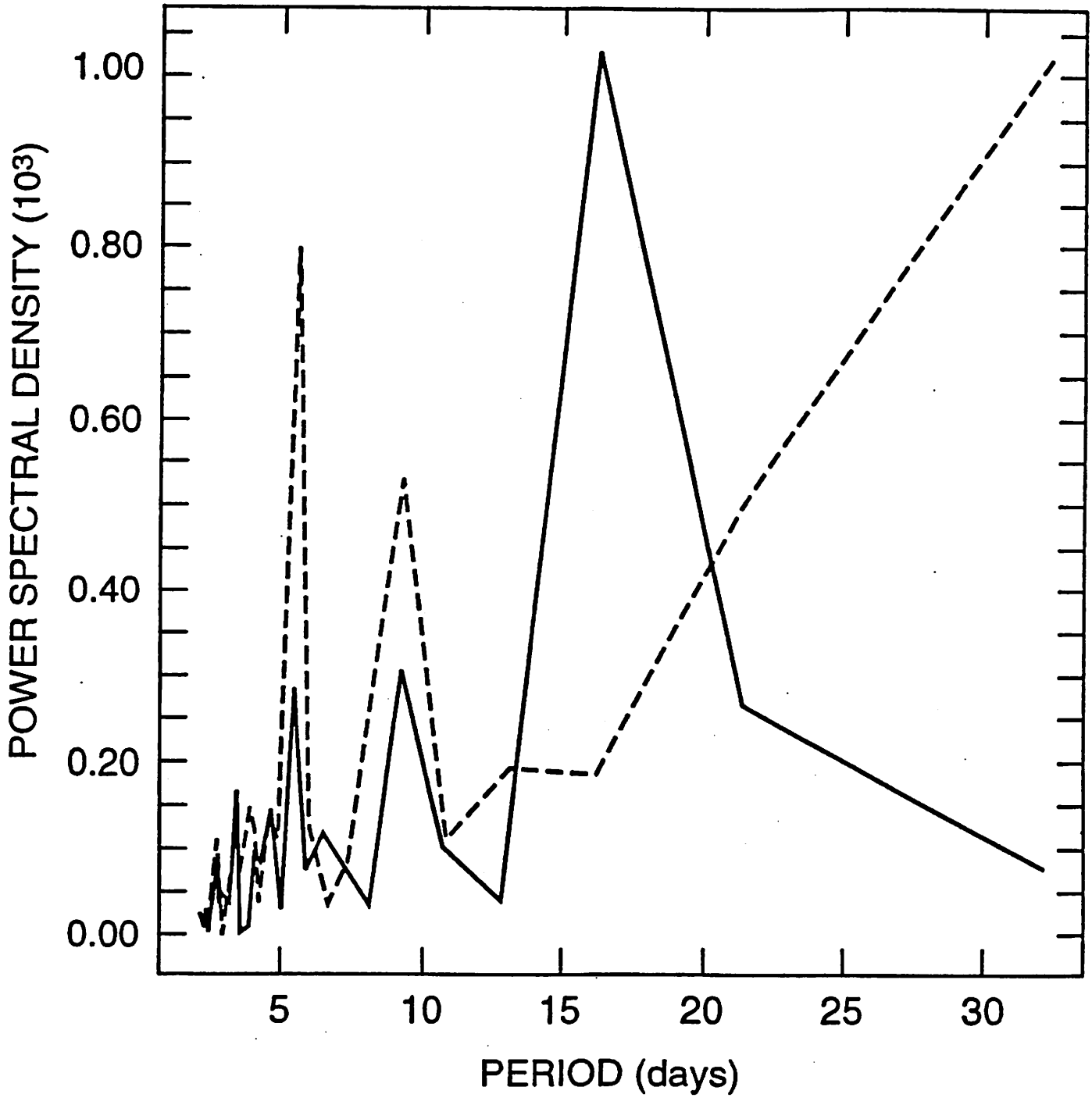

2

12507-1, 4/93, wg

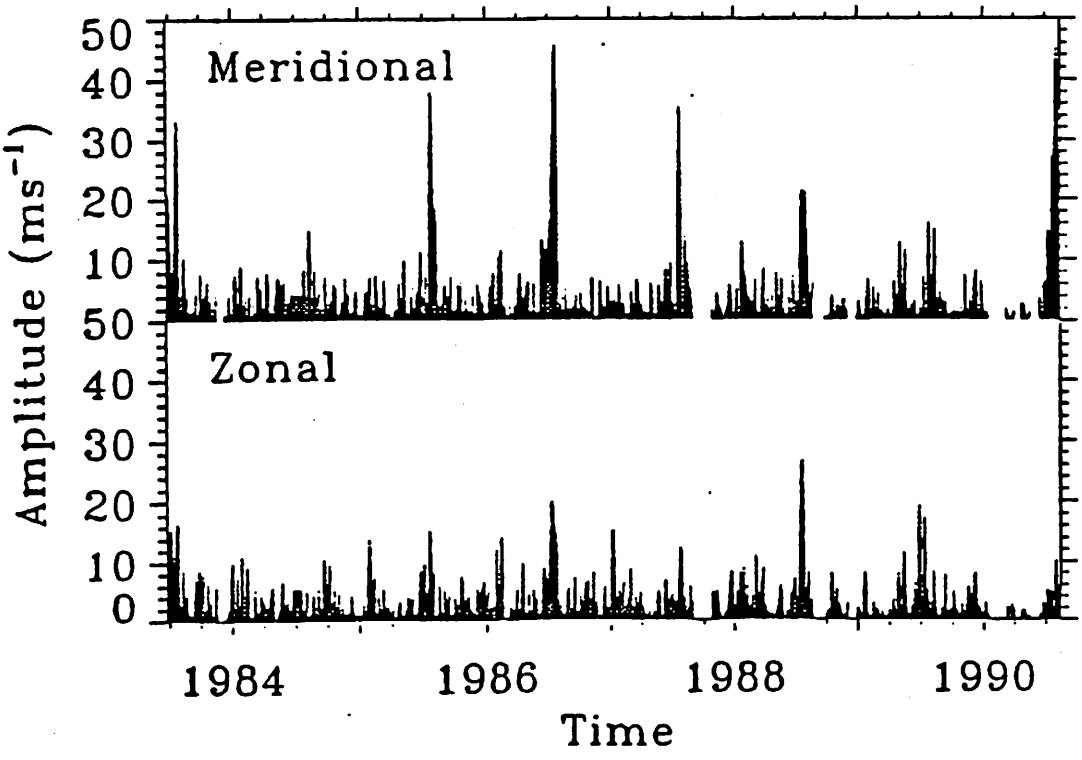
Meridional
Zonal
Amplitude (ms^{-1})
50
40
30
20
10
50
40
30
20
10
0
1984
1986
1988
1990
Time

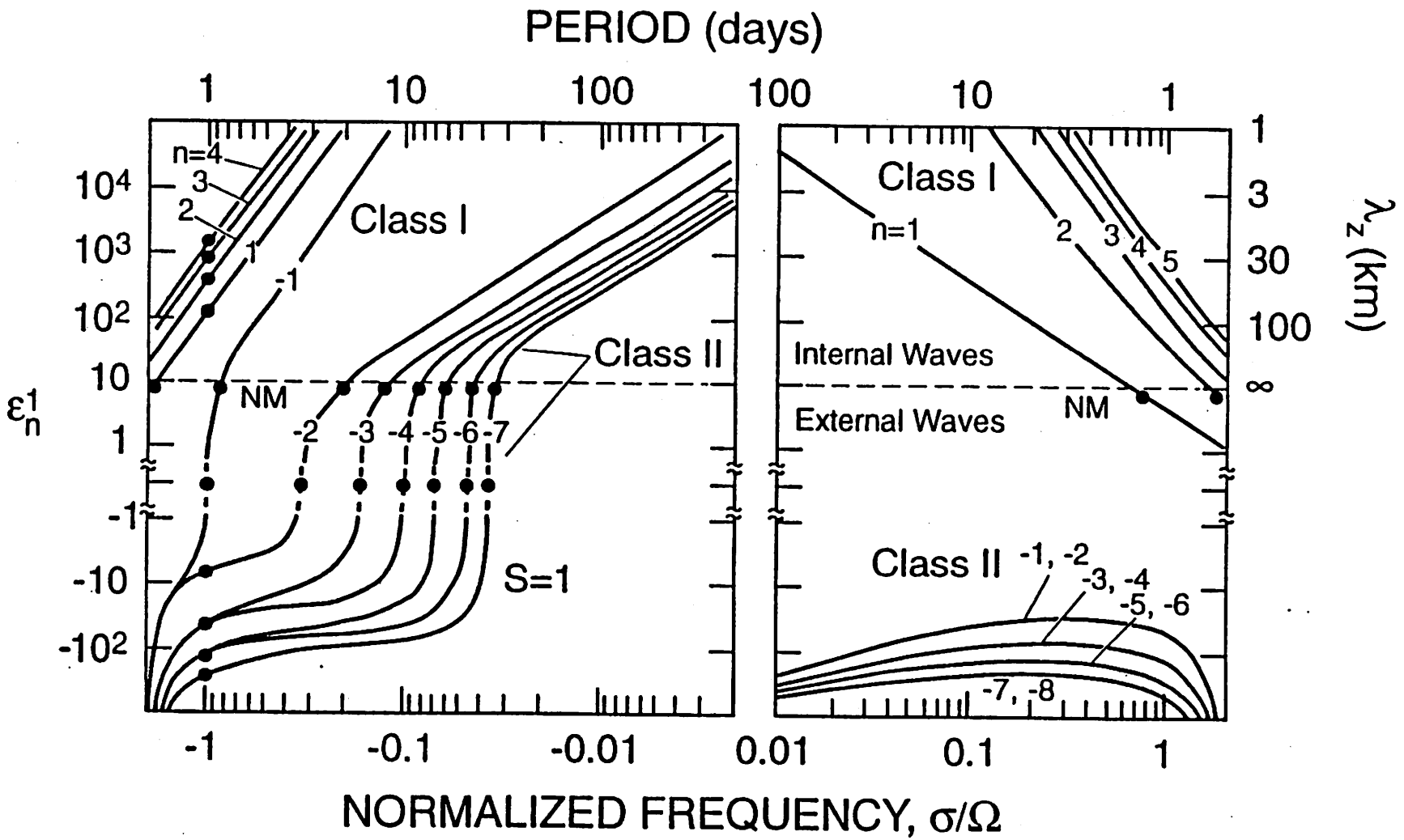

4

12507-2, 5/93, wg

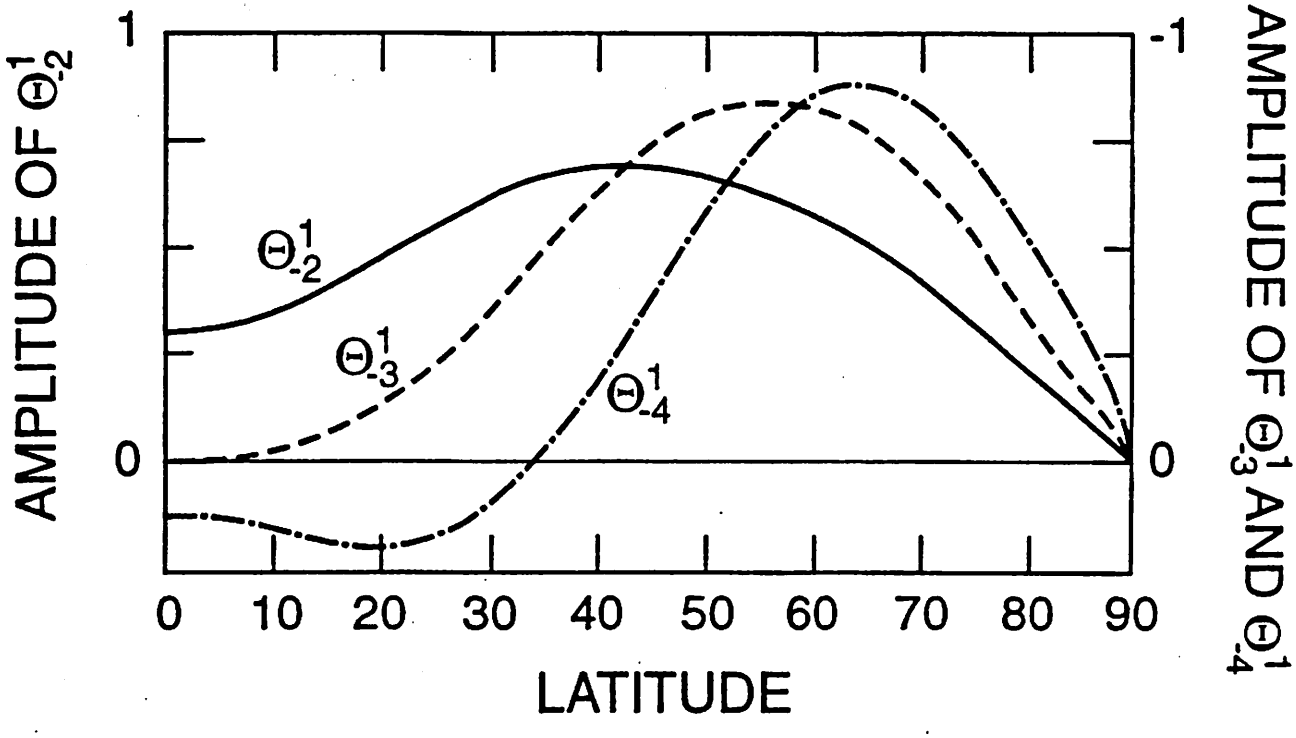

12507-4, 4/93, wg

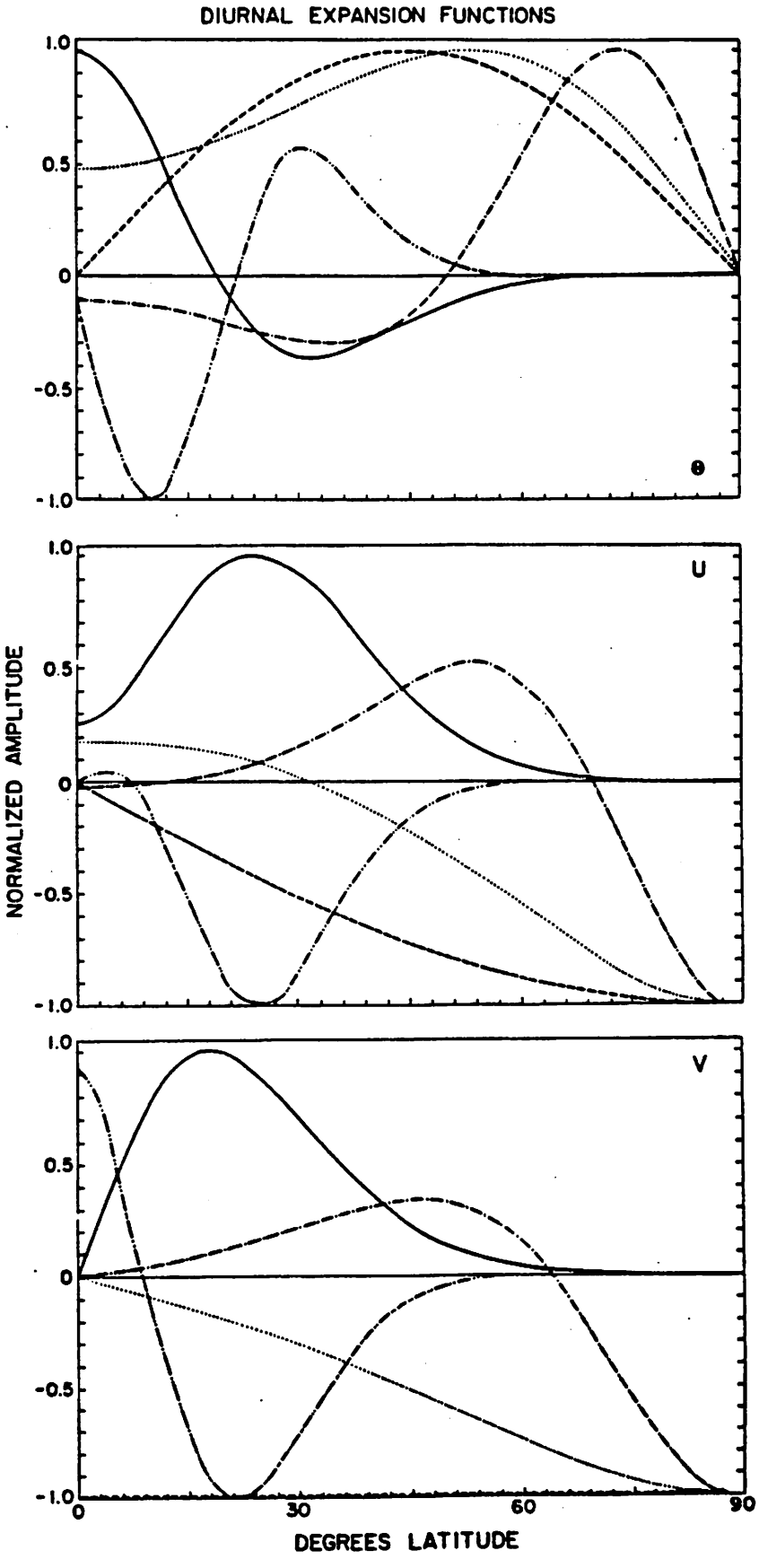
DIURNAL EXPANSION FUNCTIONS
1.0
0.5
0
-0.5
-1.0
θ
U
V
NORMALIZED AMPLITUDE
0
30
60
90
DEGREES LATITUDE

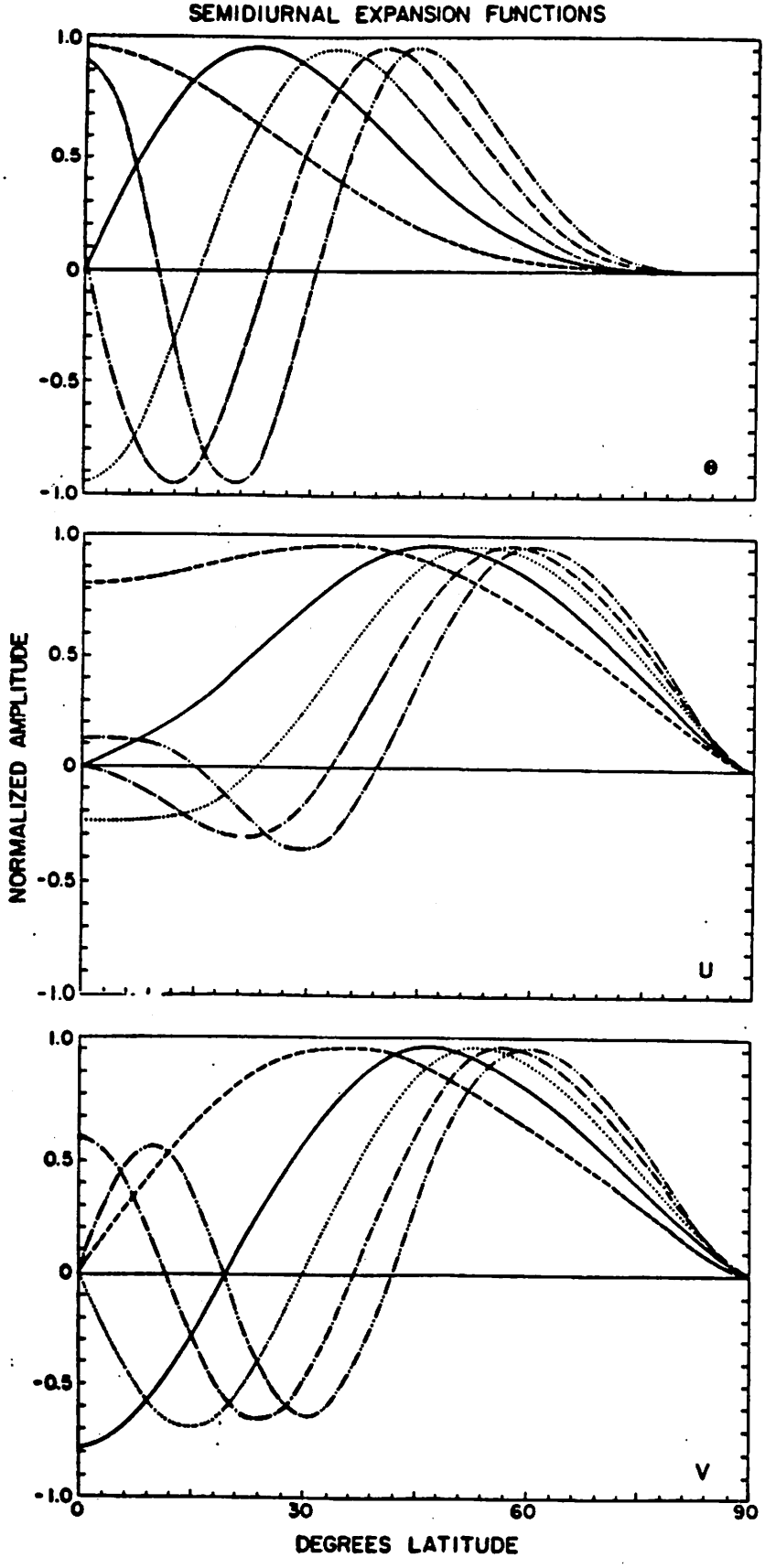
SEMIDIURNAL EXPANSION FUNCTIONS
1.0
0.5
0
-0.5
-1.0
Θ
U
V
NORMALIZED AMPLITUDE
0
30
60
90
DEGREES LATITUDE

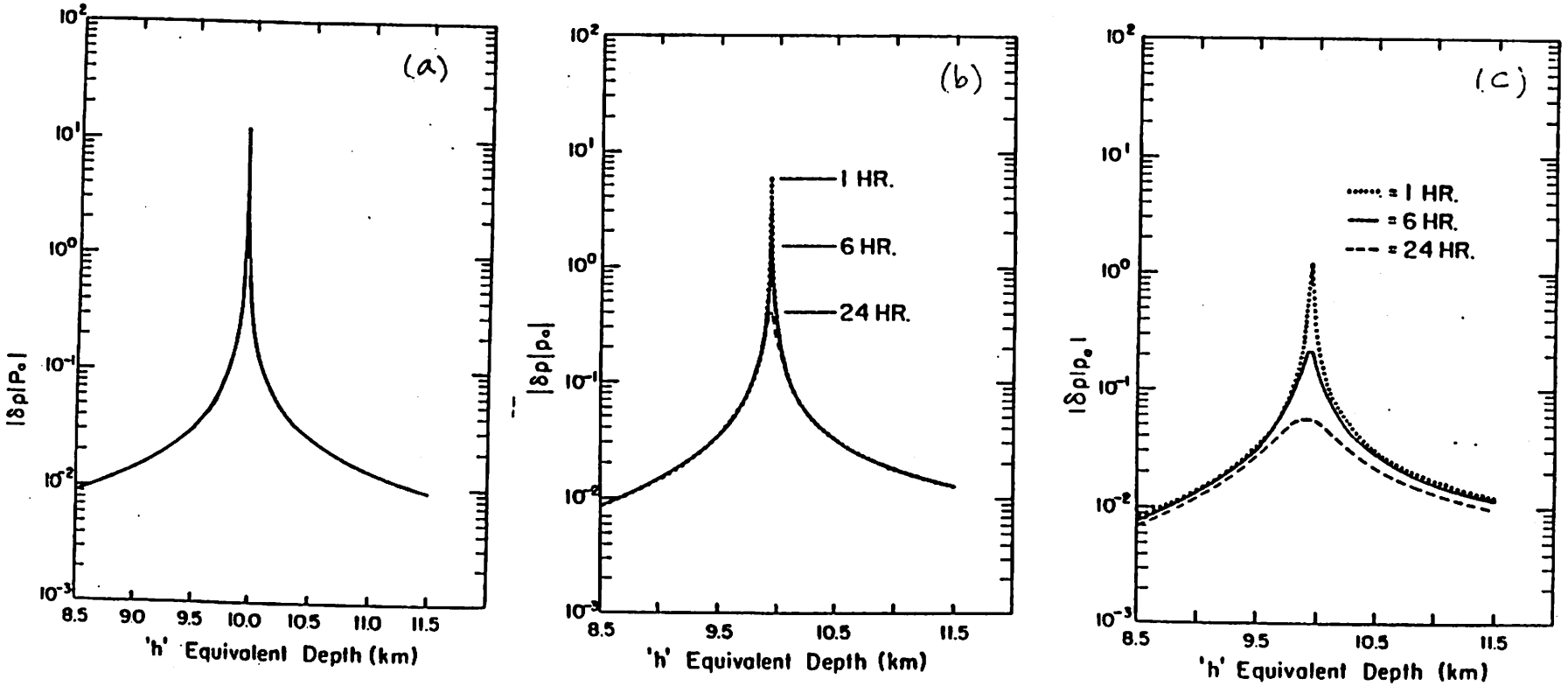
(a)
(b)
(c)
1 HR.
6 HR.
24 HR.
= 1 HR.
= 6 HR.
= 24 HR.
|δρ|ρ₀|
'h' Equivalent Depth (km)
8.5
9.0
9.5
10.0
10.5
11.0
11.5

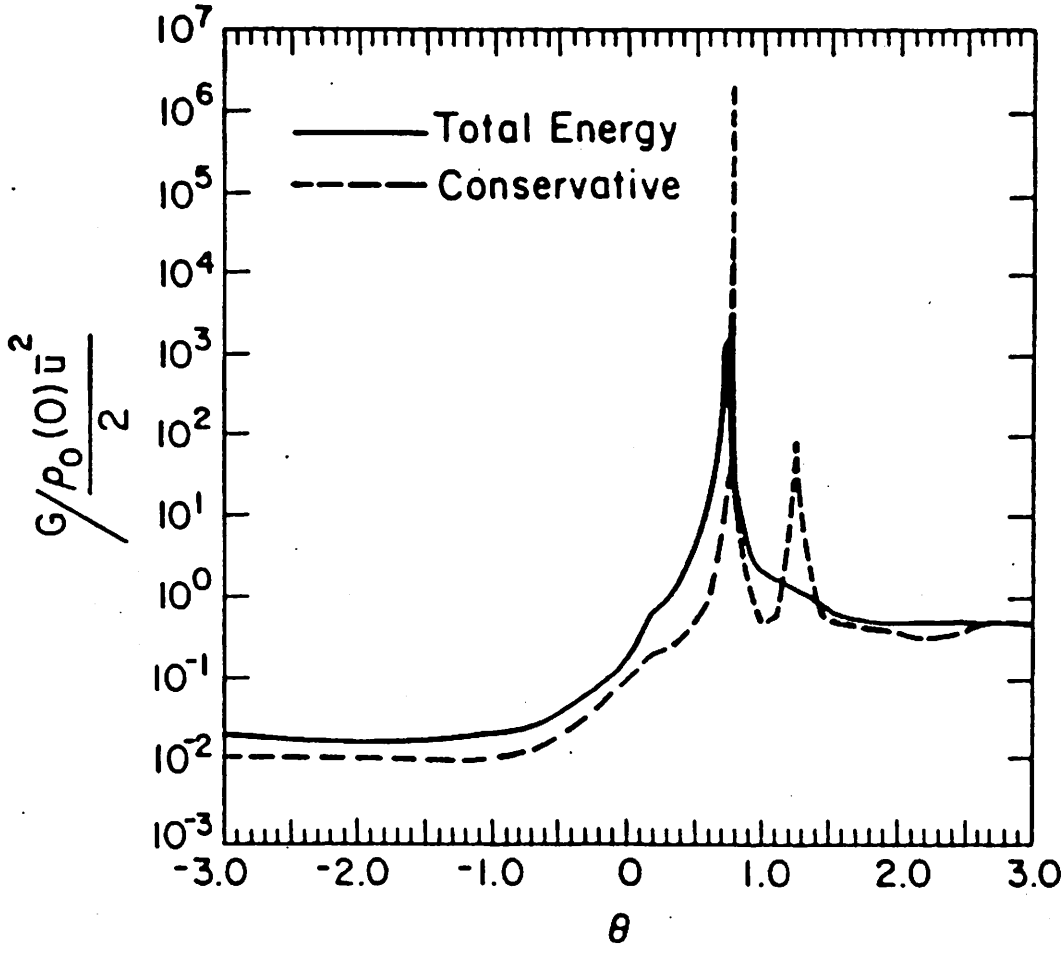
Total Energy
Conservative
$G/\frac{\rho_0(0)\bar{u}^2}{2}$
10^7
10^6
10^5
10^4
10^3
10^2
10^1
10^0
10^{-1}
10^{-2}
10^{-3}
-3.0
-2.0
-1.0
0
1.0
2.0
3.0
θ

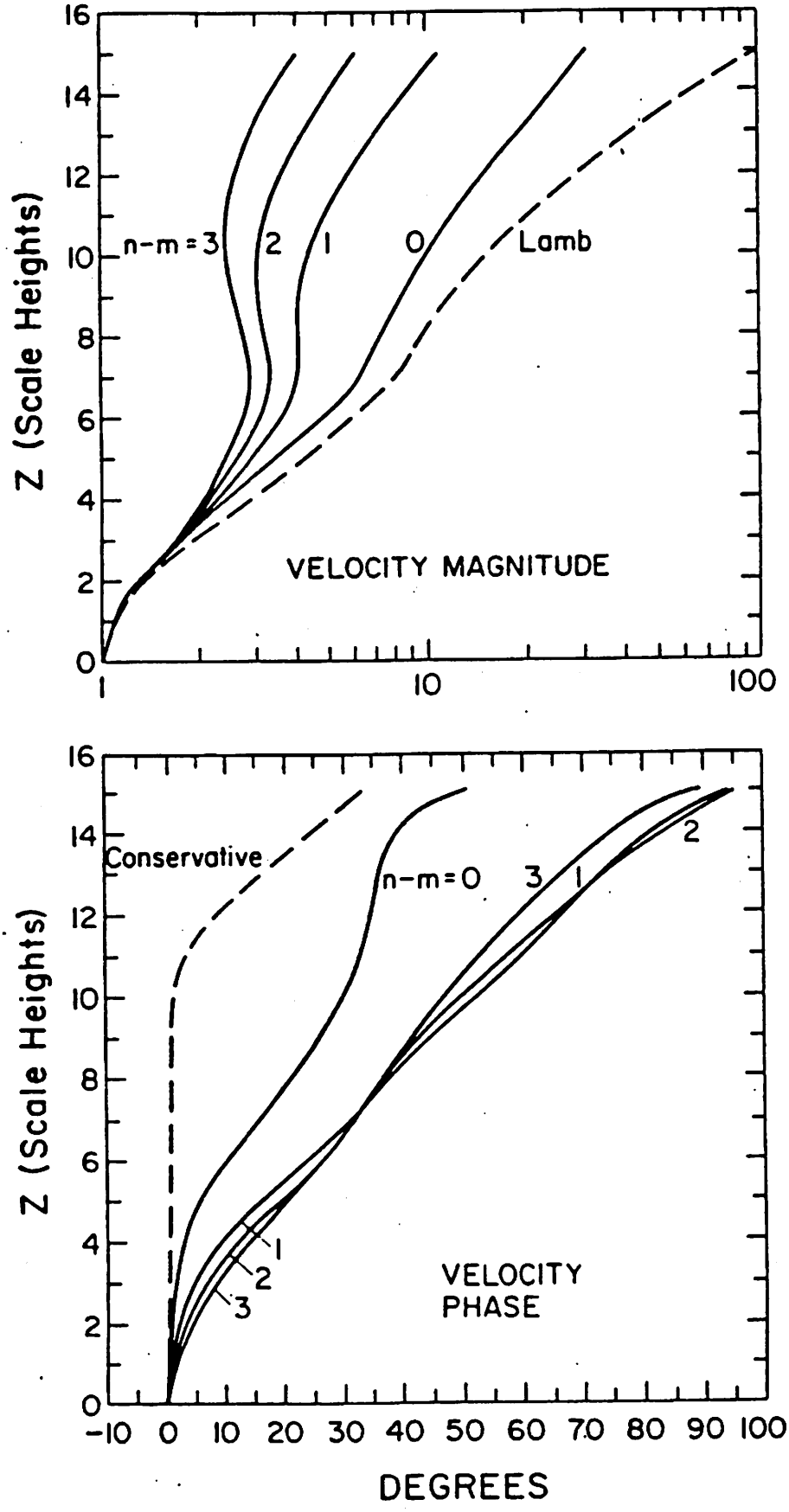
Z (Scale Heights)
n-m=3
2
1
0
Lamb
VELOCITY MAGNITUDE
1
10
100
Conservative
n-m=0
3
1
2
VELOCITY
PHASE
-10
0
10
20
30
40
50
60
70
80
90
100
DEGREES

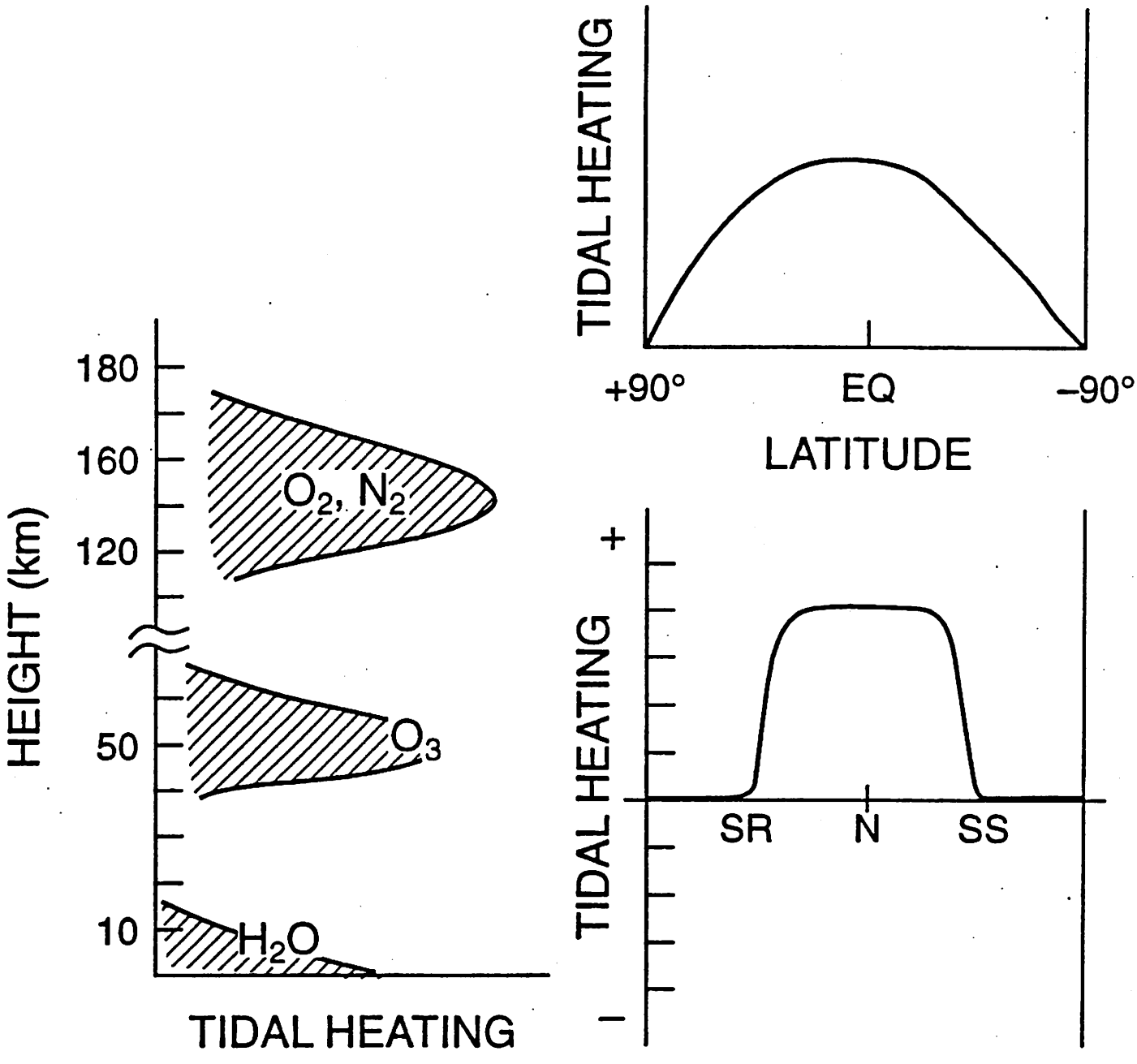

12507(fig 2), 4/93, LF

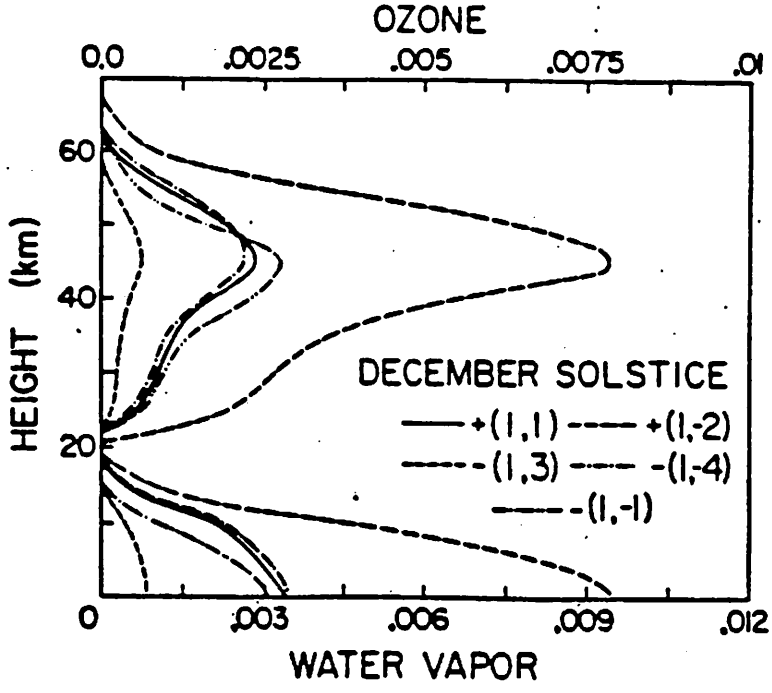
OZONE
0.0
.0025
.005
.0075
.01
60
40
20
0
HEIGHT (km)
DECEMBER SOLSTICE
+(1,1) +(1,-2)
-(1,3) -(1,-4)
-(1,-1)
.003
.006
.009
.012
WATER VAPOR

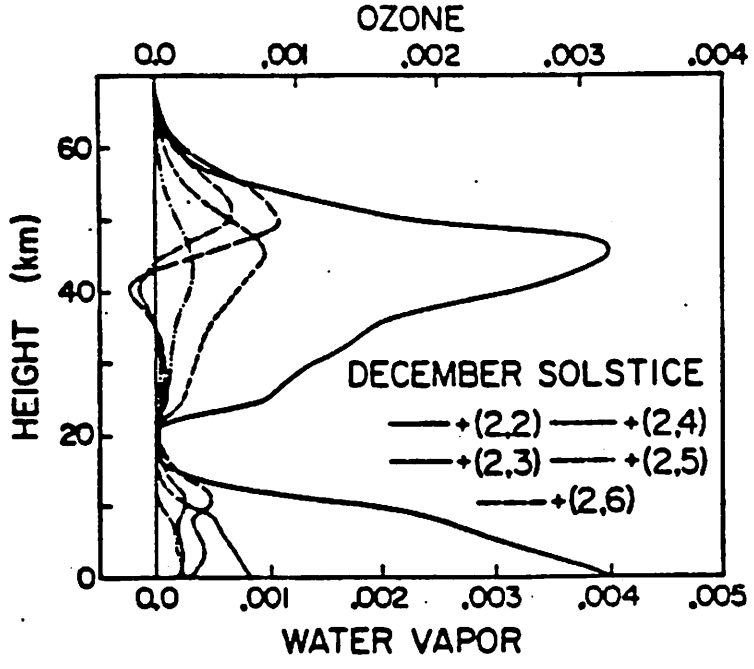
OZONE
0.0
.001
.002
.003
.004
60
40
20
0
HEIGHT (km)
DECEMBER SOLSTICE
+(2,2) +(2,4)
+(2,3) +(2,5)
+(2,6)
0.0
.001
.002
.003
.004
.005
WATER VAPOR

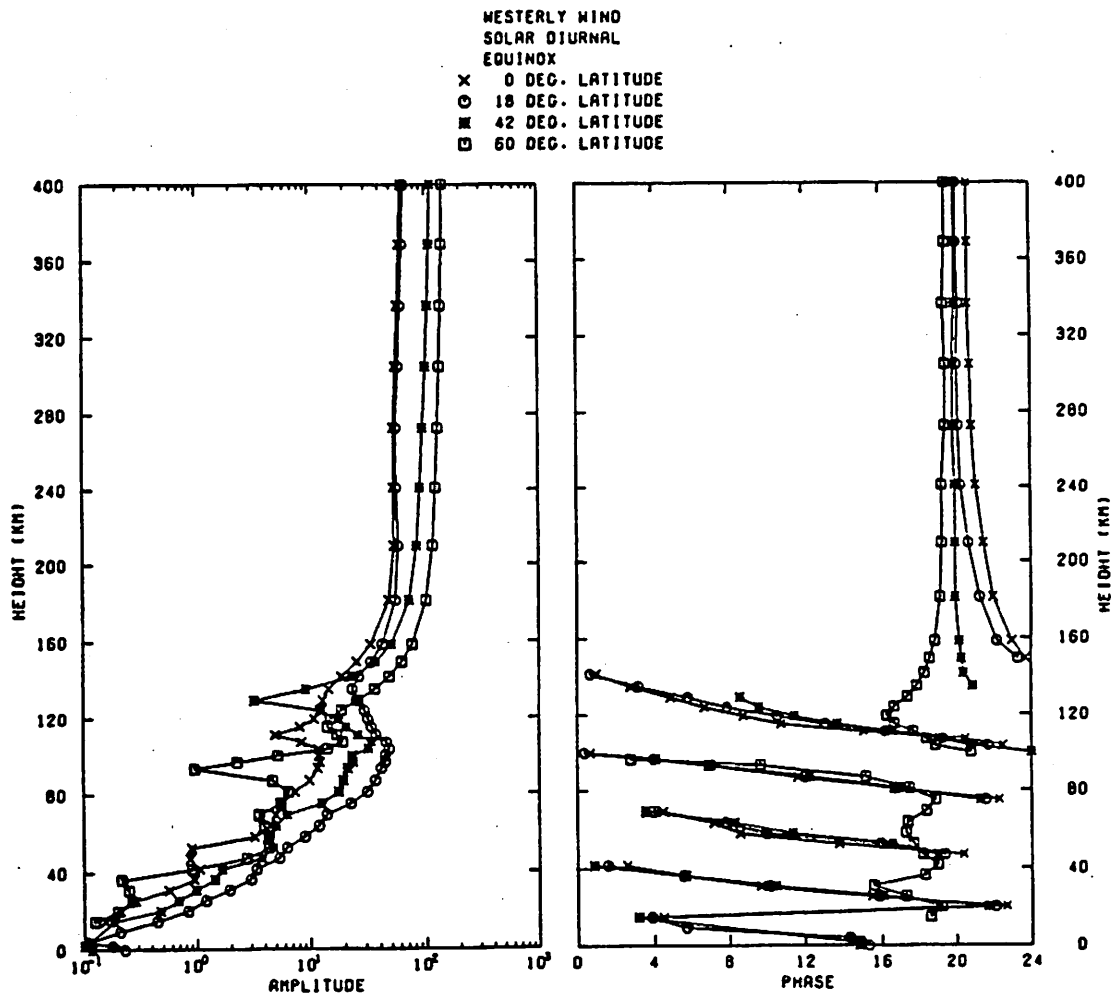
WESTERLY WIND
SOLAR DIURNAL
EQUINOX
0 DEG. LATITUDE
18 DEG. LATITUDE
42 DEG. LATITUDE
60 DEG. LATITUDE
HEIGHT (KM)
AMPLITUDE
PHASE
400
360
320
280
240
200
160
120
80
40
0
0
4
8
12
16
20
24

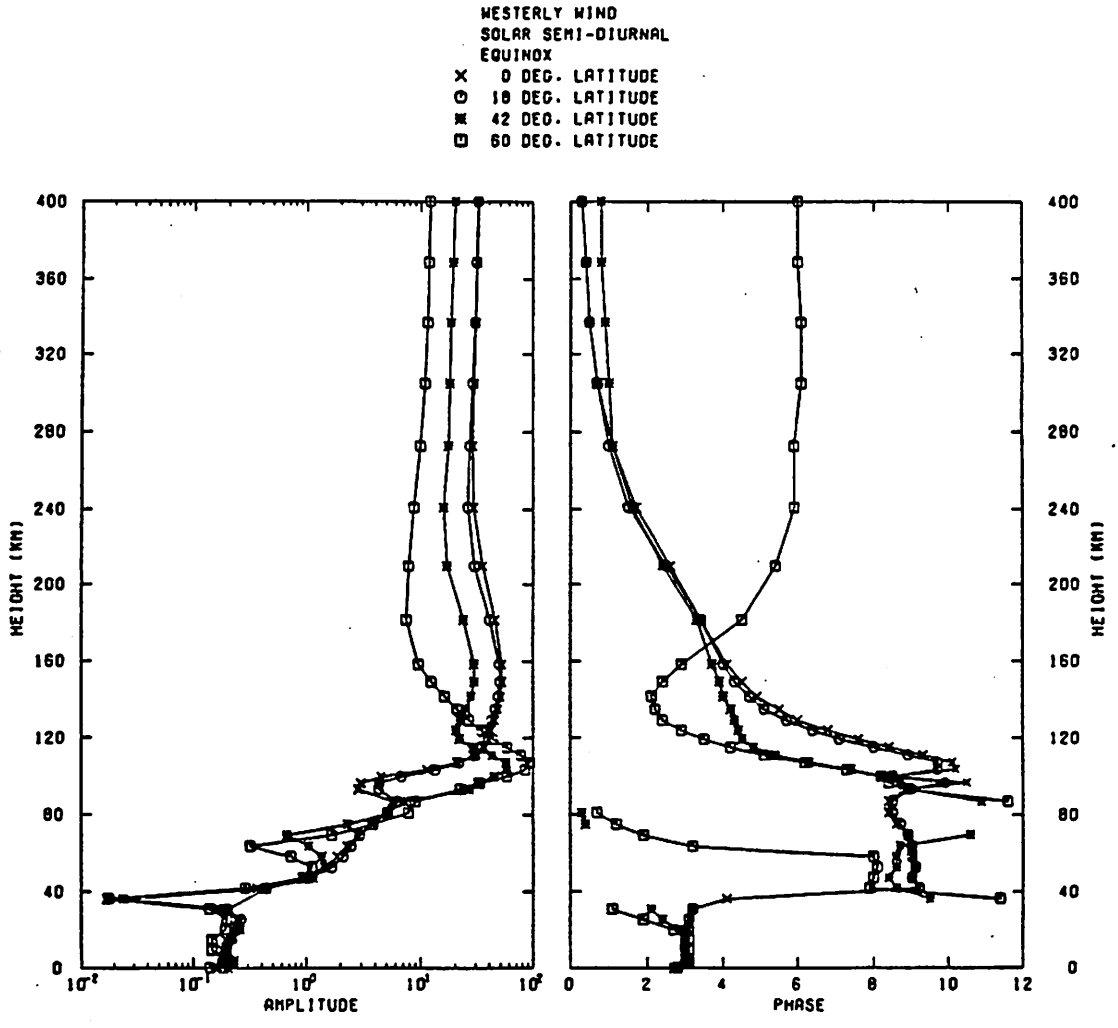
WESTERLY WIND
SOLAR SEMI-DIURNAL
EQUINOX
0 DEG. LATITUDE
18 DEG. LATITUDE
42 DEG. LATITUDE
60 DEG. LATITUDE
HEIGHT (KM)
AMPLITUDE
PHASE
400
360
320
280
240
200
160
120
80
40
0
10^{-2}
10^{-1}
10^{0}
10^{1}
10^{2}
0
2
4
6
8
10
12

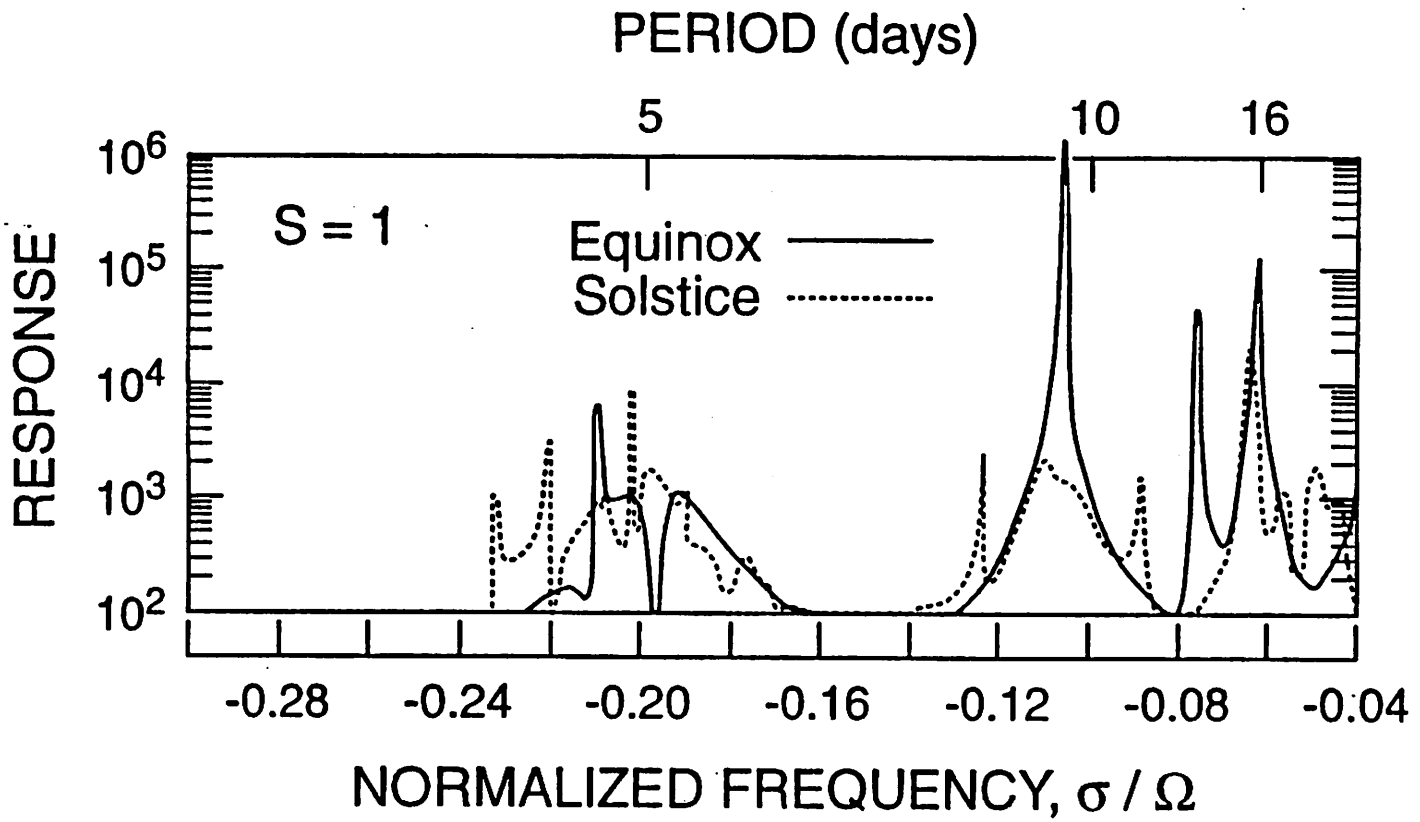

12507(Fig 3), 4/93, LF

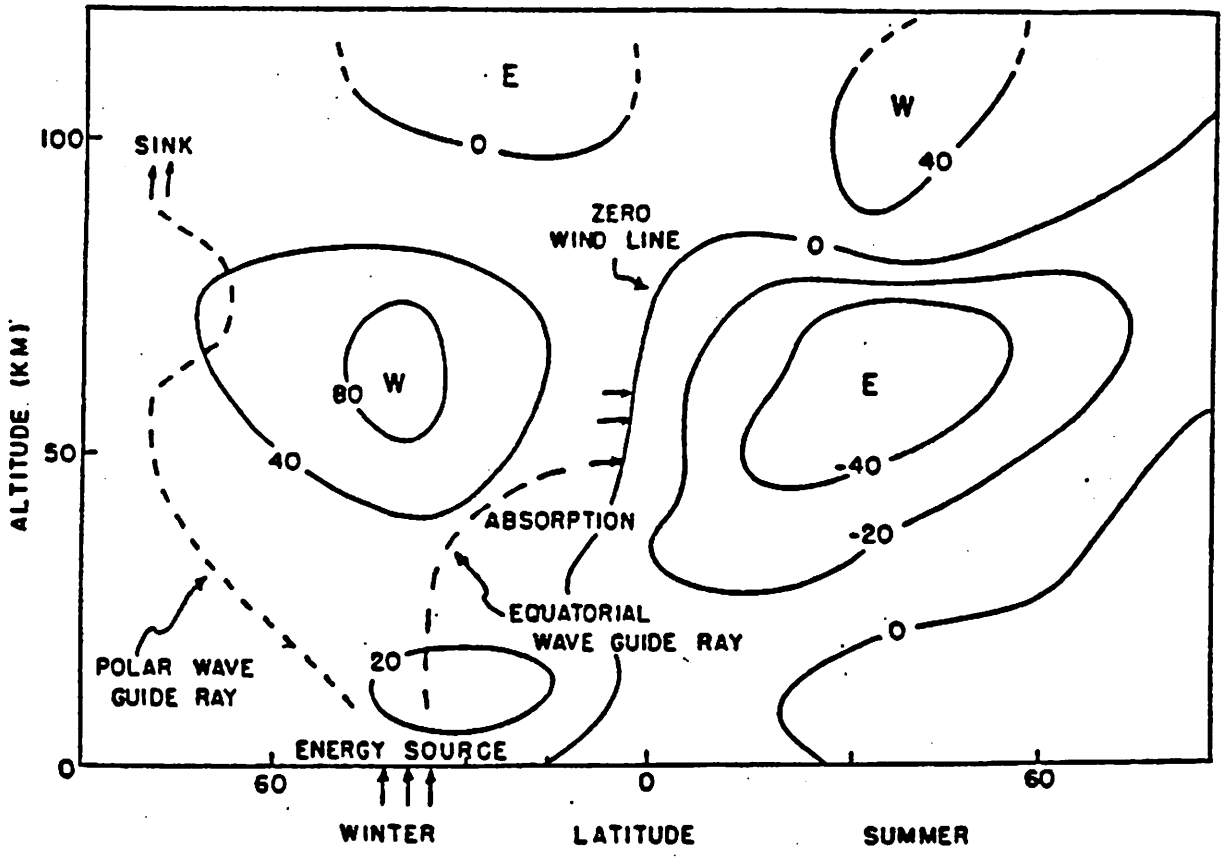
E
W
0
40
100
SINK
ZERO
WIND LINE
0
80 W
E
40
-40
50
ABSORPTION
-20
EQUATORIAL
WAVE GUIDE RAY
ALTITUDE (KM)
POLAR WAVE
GUIDE RAY
20
1
0
ENERGY SOURCE
60
0
60
WINTER
LATITUDE
SUMMER

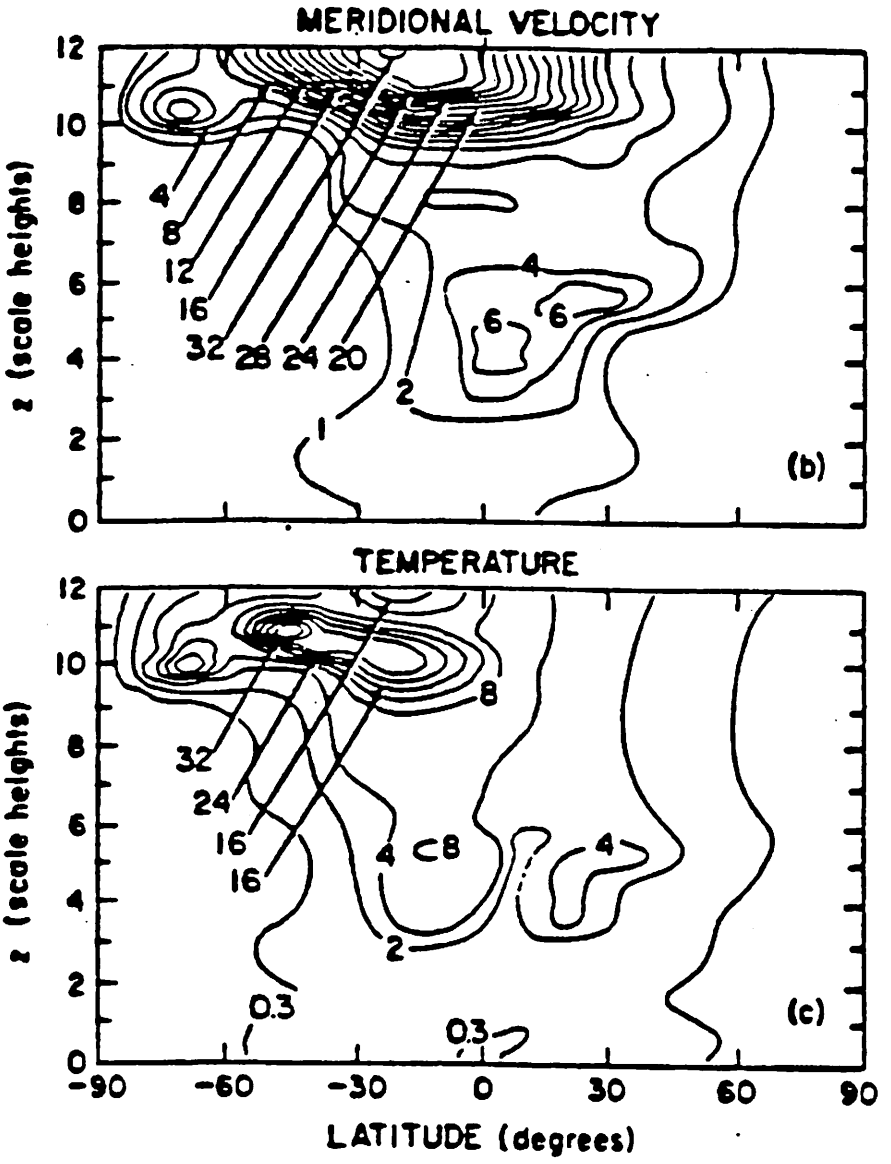
MERIDIONAL VELOCITY
z (scale heights)
12
10
8
6
4
2
0
4
8
12
16
32
28
24
20
2
1
4
6
6
(b)
TEMPERATURE
z (scale heights)
32
24
16
16
8
4
8
4
2
0.3
0.3
(c)
-90
-60
-30
0
30
60
90
LATITUDE (degrees)

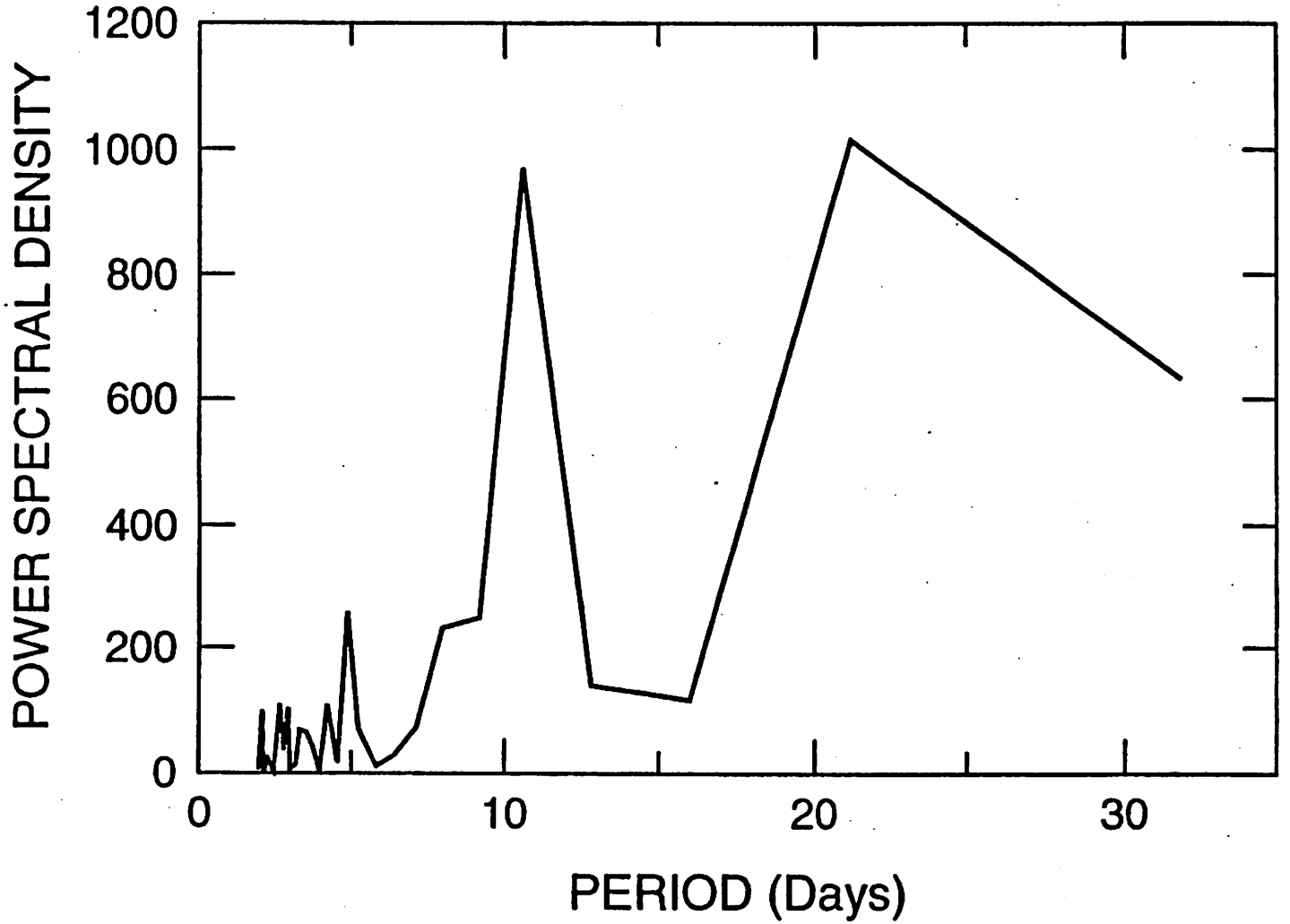

12507 fig 4/4.93 dpm